



# 1 Estimation of Evapotranspiration and Other Soil Water Budget Components in an 2 Irrigated Agricultural Field of a Desert Oasis, Using Soil Moisture Measurements

3  
4 Zhongkai Li<sup>a,b,d</sup>, Hu Liu<sup>a,b\*</sup>, Wenzhi Zhao<sup>a,b</sup>, Qiyue Yang<sup>a,b</sup>, Rong Yang<sup>a,b</sup>, Jintao Liu<sup>c</sup>

5  
6 *a. Linze Inland River Basin Research Station, Chinese Ecosystem Research Network, Lanzhou 730000, China*

7 *b. Key Laboratory of Ecohydrology of Inland River Basin, Northwest Institute of Eco-Environment and Resources, Chinese Academy of Sciences, Lanzhou, 730000, China*

8 *c. State Key Laboratory of Hydrology-Water Resources and Hydraulic Engineering, Hohai University, Nanjing 210098, China*

9 *d. University of Chinese Academy of Sciences*

10 *\* The corresponding author, [hluyz@lzb.ac.cn](mailto:hluyz@lzb.ac.cn)*

## 11 Abstract

12 An accurate assessment of soil water budget components (*SWBCs*) is necessary for improving irrigation strategies in any water-  
13 limited environment. However, quantitative information of *SWBCs* is usually challenging to obtain, because, since the hydrological  
14 process of farmland is principally driven by irrigation (*I*), drainage (*D*), and evapotranspiration (*ET*) in desert oasis settings, none  
15 of the drivers can be easily measured under actual conditions. Soil moisture is a variable that integrates the water balance components  
16 of land surface hydrology, and the evolution of soil moisture is assumed to contain the memory of antecedent hydrologic fluxes,  
17 and thus can be used to determine *SWBCs* from a hydrologic balance. A database of soil moisture measurements from six  
18 experimental plots with different treatments (NT1 to NT6) in the middle Heihe River Basin of China was used to test the potential  
19 of a soil moisture database in estimating the *SWBCs*. We first compared the hydrophysical properties of the soils in these plots, such  
20 as vertical saturated hydraulic conductivity ( $K_s$ ) and soil water retention features, for supporting the *SWBC* estimations. Then we  
21 determined evapotranspiration and other *SWBCs* through a soil-moisture data-based method that combined both the soil water  
22 balance method and the inverse Richards equation. To test the accuracy of our estimation, we used both the indirect methods (such  
23 as power consumption of the pumping irrigation well), plenty of published *SWBCs* values at nearby sites, and the water balance  
24 equation technique to verify the estimated *SWBCs* values, all of which showed a good reliability of our estimation. Finally, the  
25 uncertainties of the proposed methods were analyzed to evaluate the systematic error of the *SWBC* estimation and the restriction for  
26 its application. The results showed significant variances among the film-mulched plots (NT2-6) in both the cumulative irrigation  
27 volumes (between 652.1 mm at NT3 and 867.3 mm at NT6) and deep drainages (between 170.7 mm at NT3 and 364.7 mm at NT6).  
28 Moreover, the unmulched plot (NT1) had remarkably higher values in both cumulative irrigation volumes (1186.5 mm) and deep  
29 drainages (651.8 mm) compared with the mulched plots. Obvious correlation existed between the volume of irrigation and that of  
30 drained water. However, the *ET* demands for all the plots behaved pretty much the same, with the cumulative *ET* values ranging  
31 between 489.1 and 561.9 mm for the different treatments in 2016, suggesting that the superfluous irrigation amounts had limited  
32 influence on the accumulated *ET* throughout the growing season because of the poor water-holding capacity of the sandy soil. This  
33 work confirmed that relatively reasonable estimations of the *SWBCs* in coarse-textured sandy soils can be derived by using soil  
34 moisture measurements; the proposed methods provided a reliable solution during the entire growing season and showed a great  
35 potential for identifying appropriate irrigation amounts and frequencies, and thus a move toward sustainable water resources  
36 management, even under traditional surface irrigation conditions.

## 37 Keywords

38 Evapotranspiration, Soil water budget, Desert oasis, Soil moisture, Inverse Richards Equation.

## 39 1. Introduction

40 Arid inland river basins in Northwestern China are unique ecosystems consisting of ice and snow, frozen soil, alpine vegetation,  
41 oases, deserts, and riparian forest landscapes, in a delicate eco-hydrological balance (Liu et al., 2015). Among these inland basins,  
42 the Heihe river basin (HRB) is one of largest (Chen et al., 2007). The oasis plains in the middle reaches of the HRB have become  
43 an important source of grains, including the largest maize seed production center in China (Yang et al., 2015). Crop water  
44 requirements in this region are supplied mainly by irrigation from the river and from groundwater (Zhou et al., 2017). According to  
45 Wang et al. (2014), agriculture consumes 80 to 90% of the total water resources in the HRB, and has fundamentally altered the  
46 regional hydrological processes and even resulted in eco-environmental deterioration (Zhao and Chang, 2014). Traditional irrigation,  
47 namely flood irrigation in the HRB, has low efficiency (i.e., a high leaching fraction) (Li et al., 2017; Deng et al., 2006) and the



48 extensive fertilization practices have given rise to higher levels of potential nitrate contamination in the groundwater, because water  
49 and pollutants percolate into the deep sandy soils of the desert oasis, which have low water-holding capacities (Zhao and Chang,  
50 2014). It is crucial to adopt a mechanism that can preserve the role of irrigation in food security, yet with minimal consumption of  
51 the already scarce water, in order to increase water productivity and conservation. Reducing water drainage and thus nitrate  
52 contamination in groundwater, saving water, and increasing water and nitrogen use efficiency, are turning out to be important steps  
53 toward sustainable agriculture in this region (Hu et al., 2008)—steps that are being implemented by developing effective irrigation  
54 schedules (Su et al., 2014).

55 Because allowing the soil to dry out too much may adversely affect the yield and quality of crops, while irrigating too much  
56 can lead to wasted water, loss of fertilizer by leaching, increased operating costs and drainage problems, and sometimes decreased  
57 crop yield or quality (Wright, 1971), an efficient irrigation scheduling program should aim to replenish the water deficit within the  
58 root zone while minimizing leaching below this depth (Bourazanis et al., 2015). Accordingly, an accurate assessment of soil water  
59 budget components (*SWBCs*) is necessary for improving the irrigation management strategies in the oasis fields. However,  
60 quantitative information of *SWBCs* is usually challenging to obtain (Dejen, 2015). In desert oasis settings, the hydrological process  
61 of farmland is principally driven by irrigation (*I*), drainage (*D*), and evapotranspiration (*ET*). None of these drivers is easily measured  
62 in practice, however. For example, not even the optimal irrigation amount can be determined accurately: the two most common  
63 methods of measuring irrigation water—water meters or indirect methods—pose both economic and operational challenges to water  
64 managers, due to the wide spatial distribution of small fields throughout rural areas (Folhes et al., 2009). Measurement of deep  
65 percolation is also difficult, and reliable data are rare in practice, and thus percolation is often calculated as a residual of the water  
66 balance (Bethune et al., 2008; Odofin et al., 2012). *ET* is another source of uncertainty inherent in water budget estimations (Dolman  
67 and De Jeu, 2010), and its estimation at the field scale is usually through the application of mathematical models: it is commonly  
68 calculated by relying on reference *ET* ( $ET_0$ ) or potential *ET* (*PET*) (Allen et al., 2011; Suleiman and Hoogenboom, 2007; Wang and  
69 Dickinson, 2012; Ibrom et al., 2007).

70 Soil moisture is a variable that integrates the water balance components of land surface hydrology (Rodriguez-Iturbe and  
71 Porporato, 2005), and over time it can be used to develop a record of antecedent hydrologic fluxes (Costa-Cabral et al., 2008). Soil  
72 moisture measurements were used to estimate the infiltration for unsaturated porous mediums by numerical solutions as early as the  
73 1950s (Hanks and Bowers, 1962; Gardner and Mayhugh, 1958). With the advent of automated soil moisture monitors (Topp et al.,  
74 1980), *ET* estimation was implemented using continuous soil moisture data by simple water balance approaches (Young et al., 1997),  
75 but the computations are usually interrupted during rainfall or irrigation periods, as there is no means of accounting for drainage or  
76 recharge, due to inadequate turbulent flux measurements (Naranjo et al., 2011). It has only been during recent years that some  
77 researchers, including Schelde et al. (2011) and Guderle and Hildebrandt (2015), have started exploring the potential of using highly  
78 resolved soil moisture measurements to determine *ET* and sink term profiles, by accounting for vertical flow, demonstrating that  
79 such measurements can work when the appropriate approach is used. Rahgozar et al. (2012) and Shah et al. (2012) extended these  
80 methodologies to determine other components of the water budget, such as lateral flow, infiltration, interception capture, storage,  
81 surface runoff, and other fluxes. During the last 30 years, Time Domain Reflectometry (TDR) has become quite common and popular  
82 for measuring volumetric soil moisture content around the world (Kirnak and Akpınar, 2016). For example, it is being used more  
83 and more frequently for monitoring soil moisture dynamics of agro-ecosystems in both the Chinese Ecosystem Research Network  
84 (CERN) and the U.S. Long-Term Ecological Research Network (US-LTER) (Fu et al., 2010; Sr et al., 2003), because of its flexibility  
85 and accuracy (Schelde et al., 2011). Also, with this processes, methods based on soil moisture data have become one of the most  
86 promising ways to quantify *SWBC* information in different ecosystems (Li et al., 2010). So far, however, almost no works have been  
87 published on testing the potential of using a soil moisture database as a method to systematically estimate all the *SWBCs* of farmland  
88 in dry lands, including the desert oasis of the middle HRB (Liu et al., 2015), where the principal soils are coarse-textured (Grayson  
89 et al., 1999; Yang et al., 2018b). As one of the efforts in this region, intensive TDR measurements of soil moisture were conducted  
90 in a long-term field experiment that was originally designed to test the accumulative impacts of different cropping systems (i.e.,  
91 maize and alfalfa) and agronomic manipulation (i.e., succession cropping, crop rotation, row intercropping) on soil property  
92 evolution in the ecotones of desert and oasis. Within the context of the largest-scale deployment of soil moisture monitoring system  
93 in the world, exploring a reliable farmland *SWBC* estimation model, which can make the most of the vast amounts of soil moisture



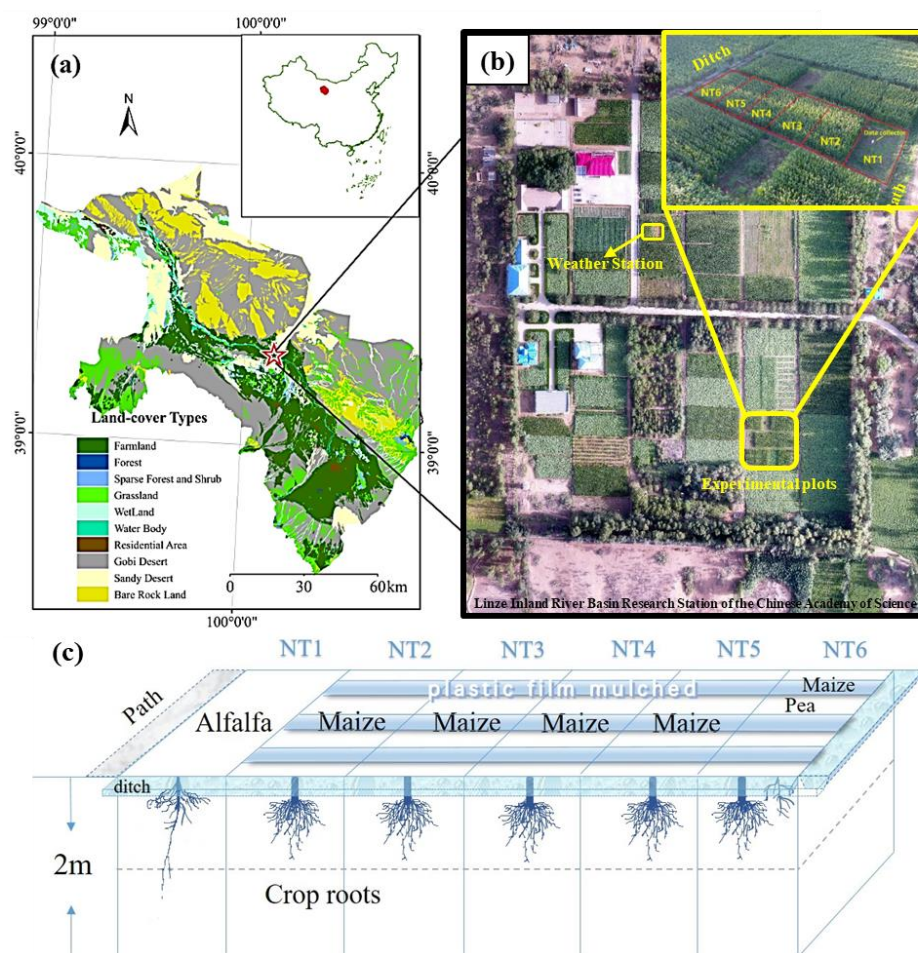
94 data, is crucial for irrigation management optimization (Musters and Bouten, 2000; Sharma et al., 2017), especially for irrigating  
95 arid regions with coarse-textured soils.

96 Based upon a soil moisture database, as mentioned above, this work aimed 1) to investigate the performance of using soil  
97 moisture measurements to determine *ET* and other *SWBCs* in the croplands of a desert oasis, serving as a framework for farmland  
98 *SWBC* estimation for coarse-textured soils; 2) to estimate the effects of different cropping systems and agronomic histories, on the  
99 hydrophysical soil properties, and to discuss these effects on the practical application of our method in different fields; and 3) to  
100 determine the potential for using a soil-moisture data-based method to improve irrigation strategies in a desert oasis.

## 101 2. Materials and Methods

### 102 2.1 Study area

103 The study sites were located in the transition zone between the Badain Jaran Desert and the Zhangye Oasis in the middle HRB  
104 (Fig. 1). More specifically, they were in the Linze Inland River Basin Research Station of the Chinese Academy of Science (39°21'N,  
105 100°17'E, altitude 1382m). This region has a temperate continental desert climate. The annual average temperature is about 7.6°C,  
106 and the lowest and highest temperatures are -27°C and 39.1°C for winter and summer, respectively. The annual average precipitation  
107 is 117 mm and the mean potential evaporation is about 2,366 mm/a. The annual dryness index is 15.9. About 60% of the total  
108 precipitation, with low rainfall intensity, is received during July–September, with only 3% occurring during winter. Northwest winds  
109 prevail throughout the year, with intense sandstorm activity in spring. This region was part of a sandstorm-eroded area, and the  
110 research site was converted into an artificial oasis during the 1970s. As a result, the soil types are dominated by sandy loam and  
111 sandy soil, and characterized by coarse texture and rapid infiltration (Zhao et al., 2010). The local dominant species are *Scotch Pine*,  
112 *Gansu poplar*, *wheat*, and *maize* (Liu et al., 2015), and sand-fixation plant species (planted since the 1970s), include *Haloxylon*  
113 *ammodendron*, *Elaeagnus angustifolia*, *Tamarix ramosissima*, *Nitraria sphaerocarpa*, and annual herbaceous species such as *Bassia*  
114 *dasyphylla*, *Halogeton arachnoideus*, *Suaeda glauca* and *Agriophyllum squarrosum*. The growing season of these plants and forages  
115 usually starts in early April and normally continues through the month of September (DOY 94-288 Julian days >0°C).



116  
 117

**Figure 1.** a) Map of study area and research site; b) aerial view of the study site; c) detailed design of the field experiments in 2016

## 118 2.2 Site description

119 In order to investigate the accumulative effect of different cropping systems and agronomic manipulation on soil property  
 120 evolution, a long-term field experiment with six different treatments was set up in 2007. The experiment was performed with  
 121 randomized complete block design (RCBD) with three replications (Figs. 1b and 1c), so that in total, 18 plots of 6m × 9m were  
 122 established. We assumed that the soil texture and cultivation history (about 40 years) of the plots subjected to the different treatments  
 123 were essentially identical before the experiment was conducted. The middle area of the three replications (6 plots, NT1 to NT6)  
 124 was selected for installing the TDR sensors. The applied treatments of NT1 to NT6 were sequentially as follows: (1) continuous pasture  
 125 cropping; (2) continuous maize cropping; (3) continuous maize cropping with straw return; (4) maize-maize-pasture rotation; (5)  
 126 maize-pasture rotation; (6) maize-pasture intercropping. Plastic film mulching was applied during the initial growing season, and  
 127 the irrigation method was furrow irrigation (Zhao et al., 2015). In 2016, NT1 was planted in alfalfa without plastic film mulch; NT2  
 128 to NT5 in maize with plastic film mulch; and NT6 in interlaced maize (mulched) and peas (non-mulched) (Fig. 1c). Maize and peas  
 129 are annual crops, and about 80% of the maize roots were distributed in the soil layers between 0 and 40 cm. only a few maize roots  
 130 can reach 100 cm, while pea roots are usually found within 30-cm depth. Alfalfa is a perennial forage legume which normally lives  
 131 four to eight years, and about 70% of alfalfa roots were distributed in the soil layers between 0 and 30 cm; only a few alfalfa roots  
 132 can reach 110 cm in the sandy soils of this region (Sun et al., 2008). The growing season of maize and alfalfa in the region is usually  
 133 from early April until late September (Zhao and Zhao, 2014). Alfalfa was harvested twice during the growing season of 2016.



134 Harvest I was conducted on 16 July, and the subsequent re-growth was harvested on 28 September (Su et al., 2010).

135 The groundwater table depth fluctuated from 5 to 8 m at the experimental field during the year 2016. Irrigation with water  
 136 extracted from a nearby pumping irrigation well was applied one by one in the plots from NT6 to NT1 during each irrigation event,  
 137 and this work was usually completed in 3 hours or less. The power consumption of the pumping irrigation well was recorded as an  
 138 in-situ observation to obtain the actual total irrigation amount of all plots through a well-built relationship at field scale: i.e., it  
 139 obtained the average actual irrigation amount of the six plots. The volumetric soil moisture of the six plots (NT1 to NT6) was  
 140 measured with a TDR system (5TE, Decagon Devices Inc. Pullman, WA, USA), which were installed at 5 different depths (20, 40,  
 141 60, 80, and 100 cm) at each plot, with measurement intervals of 10 minutes. Before use, the TDR was calibrated from soil columns  
 142 in the laboratory with known volumetric water content ( $\theta_v$ ). A maximum likelihood fitting procedure was used to correct the  
 143 observed data to eliminate the potential errors induced by the soil texture and salinity (Muñoz-Carpena, 2004). Soil bulk density  
 144 ( $\rho_b$ ), vertical saturated hydraulic conductivity ( $K_s$ ), and soil water retention were determined using standard laboratory procedures  
 145 on undisturbed soil cores in steel cylinders (110 cm<sup>3</sup> in volume, 5 cm in height) taken at 20-cm intervals down to 100-cm depth.  
 146 Soil water retention curves were measured at the pressure heads of -0.01, -0.05, -0.1, -0.2, -0.4, -0.6, -0.8, -1, -2, -5, -10, -15, -20,  
 147 and -25 bars.  $K_s$  was measured with an undisturbed soil core using the constant head method, i.e., measured 36 h after saturated  
 148 water flow at a constant head gradient (5 cm) (Salazar et al., 2008). The values of field capacity ( $\theta_{fc}$ ) and wilting point ( $\theta_w$ ) were  
 149 empirically related to the corresponding soil water (matrix) potentials through the determined soil-water retention curves (-0.1 bar  
 150 for  $\theta_{fc}$  and -15 bar for  $\theta_w$ ). Hourly climatic data, including precipitation, temperature, radiation, wind, and potential evaporation  
 151 were recorded by a weather station located about 150 meters away from the experimental site (Fig. 1).

## 152 2.3 Calculation methods

### 153 1) Water storage and irrigation amounts

154 Soil water storage ( $S$ ) was calculated for the soil depth within the root zone (0-110 cm) based on the sensor readings through  
 155 the equation:

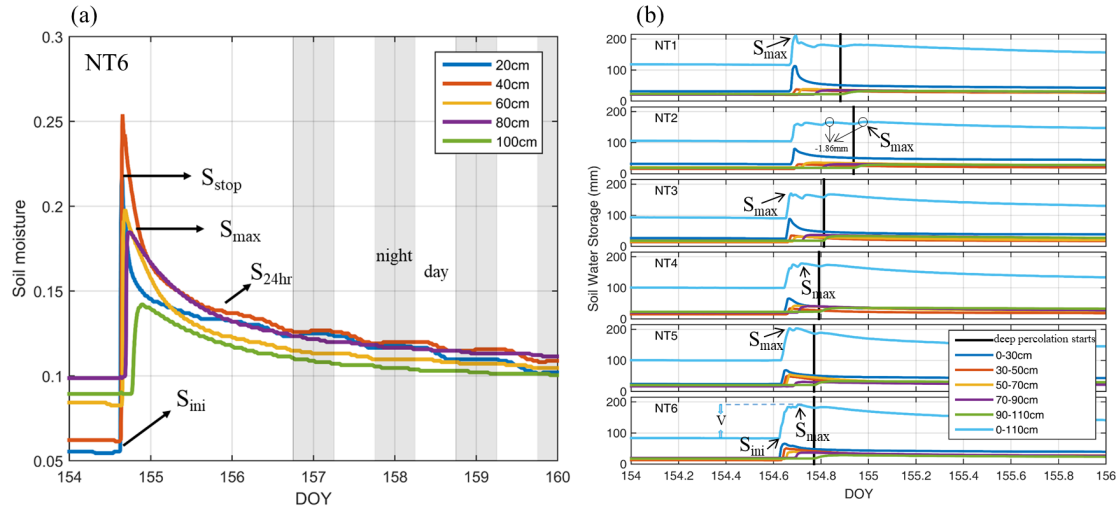
$$156 \quad S = \sum_{i=1}^5 \theta_i Z'_i \quad (1)$$

157 where  $\theta_i$  is the soil moisture of layer  $i$ ; and  $Z'_i$  is the layer thickness between 10cm above and 10cm below the sensor installation  
 158 depth (except for the top 30-cm soil layer, which is represented by the TDR installed at 20cm). At the field level, examples of  
 159 inflows are irrigation and rainfall, and examples of outflows are evaporation and deep leakage beyond the root zone. An irrigation  
 160 event usually lasted 20 to 30 minutes in each of the independent plots depending on the growth stages of the plants. Soil moisture  
 161 increased rapidly following irrigation events and decreased quickly as well during the subsequent dry-down period. Rapid drying  
 162 usually occurs for a few hours after a soil has been thoroughly wetted because of high water conductivity (Fig. 2). The preferential  
 163 flow was neglected in the selected soil profiles because the larger hydraulic conductivity of sandy soil itself neutralizes the effects  
 164 of preferential flow, and because coarse soil is relatively inimical to the formation of stable preferential flow paths (Hamblin, 1985).  
 165 Because the relatively short irrigation times that hampered the form of the steady infiltration rate (Bautista and Wallender, 1993; Selle  
 166 et al., 2011), we hypothesized that no surface-water excess or steady-state flow took place during any irrigation event, and assumed  
 167 that deep percolation began after soil moisture storage reached maximum ( $S_{max}$ ); thus the irrigation volume ( $V$ ) could be calculated  
 168 as the difference between  $S_{max}$  and  $S_{ini}$ :

$$169 \quad V = S_{max} - S_{ini} \quad (2)$$

170 where  $S_{max}$  is the maximum soil water storage of the root zone (0-110cm) after one irrigation event began and  $S_{ini}$  is the initial  
 171 soil water storage of the root zone before irrigation (Figure 2). Although the deep percolation of NT2 in this irrigation event had  
 172 begun before its soil moisture storage reached maximum (Fig. 2b), it had little effect on the estimation of irrigation volume because  
 173 the maximum soil water storage differed little (by only 1.86 mm) before and after deep percolation began. We checked all sixty of  
 174 the irrigation events of NT1-NT6 during the entire growing season period, and there were no underestimates of  $S_{max}$  except for  
 175 two irrigation events in NT2, which had a slight underestimates of 1.86 mm and 10.3 mm, which generated errors of 1.1% and 4.1%,  
 176 respectively.





177

178 **Figure 2.** (a) Example diagram of the volumetric soil water content at various depths of NT6 during and after the irrigation event of 107.1 mm on  
 179 DOY 154-160 (2016).  $S_{stop}$ : irrigation event ends, and moisture of uppermost soil layer starts to decrease;  $S_{max}$ : maximum water storage;  $S_{24hr}$ :  
 180 deep percolation ends one day later; after this point, ET dominates the water-loss processes;  $S_{ini}$ : pre-irrigation, soil moisture minimum. The gray  
 181 stripes between 156-160 DOY represent nights, i.e., 6:00 pm to 6:00 am of the next day. (b) Verification of the assumption of equation 2, i.e., that  
 182  $S_{max}$  appeared before deep percolation began, during the irrigation event on DOY 154-156 (2016). The black solid line represents the time that  
 183 deep percolation began in each plot (NT1-6).

## 184 2) Drainage and evapotranspiration

185 Following irrigation water applications, the drainage behavior of the soils consisted of two stages: 1) rapid drainage and 2)  
 186 slow drainage. During irrigation, the root zone became effectively saturated, and rapid drainage followed, leading to deep percolation.  
 187 Then, as the water content in the soil fell, the hydraulic conductivity decreased sharply, as did the rate of drainage. The second phase,  
 188 slow drainage, may continue for several days or months, depending on the soil texture (Bethune et al., 2008). We assumed that rapid  
 189 drying or drainage ceased 24 hours after an irrigation event, and thus rapid drainage ( $Q_1$ ) could be estimated through the variances  
 190 of water storage and actual ET during the period (Eq. 3). The actual ET during the period was assumed to be equal to the potential  
 191 ET, because ET occurs unhindered under non-water-stress conditions.

192

$$192 \quad Q_1 = S_{max} - S_{24hr} - ET_p \quad (3)$$

193

193 where  $S_{24hr}$  is the soil moisture storage 24 hours after irrigation;  $S_{max}$  is the maximum water storage after irrigation; and  $ET_p$   
 194 is the potential ET calculated with the Penman-Monteith combination equation during that day.

195

195 Slow drainage is especially important for sandy soils (Bethune et al., 2008), as along with ET, it dominates the water loss  
 196 processes during the second drying stage before the next irrigation event. Following Zuo et al. (2002) and Guderle and Hildebrandt  
 197 (2015), an inverse method was employed to estimate the slow drainages and the average root water uptakes by solving the mixed  
 198 theta-head formulation of the 1-D Richards Equation (Eq. 4) and iteratively searching for the sink term profile that produces the  
 199 best fit between the numerical solution and the measured values of soil moisture content. ET is then obtained by summing rainfall  
 200 and the sink term ( $S_p$ ), and the drainage for this period is estimated as the water flux across the lower boundary of the soil profile.  
 201 The above-mentioned 1-D Richards Equation is written as:

202

$$202 \quad C(h) \frac{\partial h}{\partial t} = \frac{\partial}{\partial t} \left[ K(h) \left( \frac{\partial h}{\partial z} - 1 \right) \right] - S_p(z, t); \quad (4)$$

203

$$203 \quad h(z, 0) = h_0(z) \quad 0 \leq z \leq L; \quad (5)$$

204

$$204 \quad \left[ -K(h) \left( \frac{\partial h}{\partial z} - 1 \right) \right]_{z=0} = -E(t) \quad t > 0; \quad (6)$$

205

$$205 \quad h(L, t) = h_l(t) \quad t > 0; \quad (7)$$

206

206 where  $h$  is the soil matric potential (cm);  $C(h)$  the soil water capacity ( $\text{cm}^{-1}$ );  $K(h)$  the soil hydraulic conductivity ( $\text{cm d}^{-1}$ );  $h_0(z)$  the  
 207 initial soil matric potential in the profile (cm);  $E(t)$  the soil surface evaporation rate (cm);  $h_l(t)$  the matric potential at the lower  
 208 boundary (cm);  $L$  the simulation depth (cm); and  $z$  the vertical coordinate originating from the soil surface and moving positively



209 downward (cm). The iterative procedure runs the numerical model over a given time step ( $\Delta t$ ) in order to estimate the soil water  
 210 content profile  $\tilde{\theta}_i^{v=0}$  at the end of the time step, assuming that the sink term  $\tilde{S}p_{im,i}^{(v=0)}$  is zero over the entire profile at the beginning,  
 211 where  $\sim$  depicts the estimated values at the respective soil layer  $i$ , and  $v$  indicates the iteration step. Next, the sink term profile  
 212  $\tilde{S}p_{im,i}^{(v=1)}$  is set equal to the difference between the previous approximation  $\tilde{\theta}_i^{v=0}$  and the measurements  $\theta_i$ , while accounting for  
 213 soil layer thickness and the length of the time step for units. In the following iterations,  $\tilde{S}p_{im,i}^{(v)}$  was used with the Richards equation  
 214 to calculate the new soil water content  $\tilde{\theta}_i^v$ . The new average sink term  $\tilde{S}p_{im,i}^{(v+1)}$  was then determined with Eq. (8):

$$215 \quad \tilde{S}p_{im,i}^{(v+1)} = \tilde{S}p_{im,i}^{(v)} + \frac{\tilde{\theta}_i^v - \theta_i}{\Delta t} \cdot d_{z,i}; \quad (8)$$

216 A backward Euler with a modified Picard iteration finite differencing solution scheme was adopted to inversely obtain the  
 217 solution, and this implementation follows exactly the algorithm outlined by Celia et al. (1990). Three steps proposed by Guderle  
 218 and Hildebrandt (2015) were taken to determine when the iteration process could be terminated in this calculation:

219 a. Evaluate the difference between the estimated and measured soil water contents (Eq. 9) and compare the change in this  
 220 difference to the difference from the previous iteration (Eq. 10):

$$221 \quad e_i^{(v)} = |\theta_i - \tilde{\theta}_i^v| \quad (9)$$

$$222 \quad \varepsilon_{GH,i}^{(v)} = |e_i^{(v-1)} - e_i^{(v)}| \quad (10)$$

223 b. In soil layers where  $\varepsilon_{GH}^{(v)} < 0$ , set the root water uptake rate back to the value of the previous iteration  $\tilde{S}p_{im,i}^{(v+1)} = \tilde{S}p_{im,i}^{(v-1)}$ , since  
 224 the current iteration was no improvement. Only if  $\varepsilon_{GH}^{(v)} \geq 0$ , go to the next step.

225 c. If  $e_i^{(v)} > 1 \times 10^4$ , calculate  $\tilde{S}p_{im,i}^{(v+1)}$  according Eq. (8); otherwise the current iteration sink term ( $\tilde{S}p_{im,i}^{(v+1)} = \tilde{S}p_{im,i}^{(v)}$ ) is retained,  
 226 as it results in a good fit between estimated and measured soil water content.

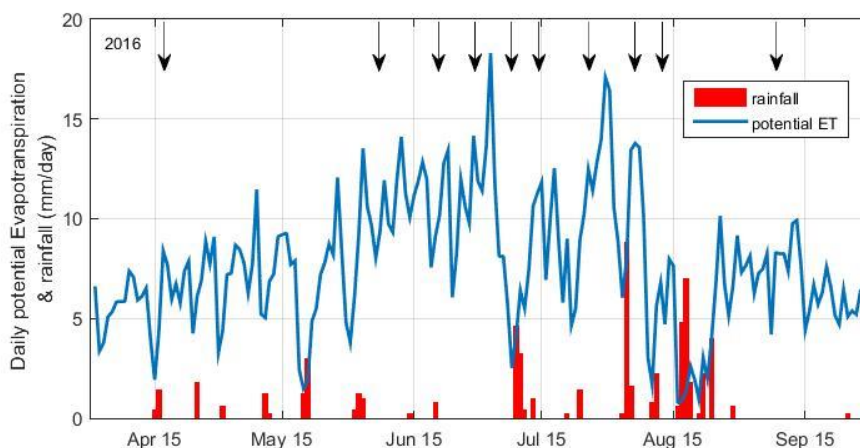
### 227 3) Boundary setting and data collection

228 To reduce computational complexity, uniform soil profiles were assumed because there were no significant stratification  
 229 differences within the sandy soils (Table 2) (Liu et al., 2015). The upper boundary of the calculation was set as the atmospheric  
 230 boundary condition, and the calculation involved actual precipitation, irrigation, and potential evapotranspiration rates calculated  
 231 through Penman-Monteith combination equations using hourly environmental data during the growing season of 2016 (Fig. 3). The  
 232 meteorological measurements were monitored at the nearby weather station (150 m away from our study plots, Fig. 1), which had  
 233 the same underlying surface as the experimental plots (Fig. 1b), and were used to compute the upper boundary condition. The film  
 234 mulching effects on the upper boundary condition were modeled as proportionally damped  $ET_{p,a} = \beta \times ET_p$ , where  $\beta$  is the area  
 235 percentage without plastic film mulching in each experimental plot (i.e., 60%), and  $ET_p$  is the potential ET. For coding convenience,  
 236 the bare soil evaporation ( $E_a$ ) was determined through a simplified method proposed by Porporato et al. (2002): i.e., the evaporation  
 237 was assumed to linearly increase with soil moisture ( $\theta$ ) from 0 at the hygroscopic point ( $\theta_h$ ), to  $E_{p,a}$  at the field capacity ( $\theta_{fc}$ ). For  
 238 values  $\theta$  exceeding the field capacity, evapotranspiration was decoupled from soil moisture and remained constant at  $E_{p,a}$ .  
 239 However, we did not set specific upper boundaries for inter-cropping treatments, because the difference in surface soil evaporation  
 240 between mono- and inter-cropping treatments was relatively small when compared with the transpiration over a growing season.  
 241 The surface fluxes were incorporated by using the average hourly rates, distributed uniformly over each hour. The lower boundary  
 242 condition was set as a soil matric potential boundary because the groundwater table depth (deeper than 3.5 m) was far below the  
 243 crop effective root depth during the growing season, and any capillary rise from groundwater could be ignored in this study. A  
 244 vertical hydraulic gradient boundary condition (i.e.,  $h = -5\text{cm}$ ) was implemented in the simulation in the form of a variable flux  
 245 boundary condition. The drainage rate  $q(n)$  assigned to the bottom node  $n$  was determined by the software as  $q(n) = -K(h)$ , where  
 246  $h$  is the local value of the pressure head and  $K(h)$  is the hydraulic conductivity corresponding to this pressure head (Odofin et al.,  
 247 2012).

248 We used soil moisture dynamics measured in the soil profiles as inputs to inversely solve for sink term profiles at each plot for  
 249 each hour (Lv, 2014). The soil moisture measurements for 10-minute intervals during the period were hourly averaged to numerically  
 250 filter out the noise associated with highly resolved data. This had the effect of slightly reducing the infiltration and ET estimates,  
 251 but this effect in the overall results is negligible, according to Guderle and Hildebrandt (2015). The actual amount of water delivered  
 252 for irrigation ( $Q_0$ ) was determined from the power consumption of water pumping ( $P_0$ ), through a relationship established between  
 253 the two:  $Q_0 = P_0 \times \eta$ , where  $\eta$  is the ratio of the power consumption per unit water pumped and is likely to be different for  
 254 different pumping heads. The coefficient was experimentally determined to be  $8.5 \text{ m}^3 \text{ kW}^{-1} \text{ h}^{-1}$  for a head corresponding to 0.95



255 kg/cm<sup>2</sup> of delivery pressure, in this study.



256

257

**Figure 3.** Measured daily rainfall and potential ET estimated with the Penman-Monteith method during the growing season of 2016 at Linze Station. The cumulative rainfall during the growing season was 69.2mm in 2016, and the black down arrows represent irrigation events.

258

259

260

**Table 1.** Nomenclatures involved in this study

$V$	irrigation amount for one irrigation event (mm)	$K(h)$	soil hydraulic conductivity (cm d <sup>-1</sup> )
$S$	soil water storage (mm)	$h_0(z)$	initial soil matric potential in the profile (cm)
$S_{stop}$	soil moisture storage when irrigation was stopped (mm)	$E(t)$	soil surface evaporation rate (cm)
$S_{ini}$	soil moisture storage before irrigation start (mm)	$h(t)$	matric potential at the lower boundary (cm)
$S_{24hr}$	soil moisture storage 24 hours after irrigation (mm)	$L$	simulation depth (cm)
$S_{max}$	maximum soil water storage during irrigation event (mm)	$z$	vertical coordinate originating from the soil surface and moving positively downward (cm)
$\theta_i$	volumetric soil water content of layer $i$	$\bar{\theta}_i^{v=0}$	soil water content profile of soil layer $i$ at the beginning of each calculation
$\theta_v$	theoretical volumetric water content calculated by the ratio of soil volume to water volume	$\bar{S}_{p_{im,i}}^{(v=0)}$	sink term of soil layer $i$ at the beginning of irrigation, assuming it is zero
$\eta$	ratio of the power consumption per unit water pumped	$d_{z,i}$	thickness of soil layer $i$
$t$	time	$\sim$	estimated values at soil layer $i$
$Q$	steady-state drainage (mm)	$v$	iteration step
$ET_p$	potential ET during irrigation day (mm)	$\bar{\theta}_i^v$	soil water content of step $v$
$Z'_i$	detection range of TDR, i.e., 20 cm	$\bar{S}_{p_{im,i}}^{(v)}$	average sink term of step $v$
$S_p$	sink term, i.e., water extraction by roots, evaporation, etc. (cm)	$\Delta t$	given time step
$h$	soil matric potential (cm)	$e_{GH,i}^{(v)}$	difference between $e_i^{(v-1)}$ and $e_i^{(v)}$
$C(h)$	soil water capacity (cm <sup>-1</sup> )	$e_i^{(v)}$	difference between estimated and measured soil water content
$Q_0$	real amount of water delivered for irrigation (m <sup>3</sup> )	$P_0$	power consumption (kWh)
$D_{seas}$	theoretical drainage volume over entire growing season in 2016 (mm)	$R_{seas}$	cumulative rainfall during entire growing season in 2016 (mm)
$V_{seas}$	theoretical irrigation volume over entire growing season in 2016 (mm)	$ET_{seas}$	theoretical ET volume during entire growing season in 2016 (mm)
$\Delta S$	difference in soil water storage before and after the growing season (mm)	$\rho_b$	soil bulk density (g/cm <sup>3</sup> )
$K_s$	saturated water conductivity (cm/day)	$\theta_s$	saturated water content
$\theta_{fc}$	field capacity	$\theta^*$	water stress point
$\theta_w$	wilting point	$\Psi$	soil water (matric) potential
$\theta_h$	hygroscopic point	$\beta$	the area percentage without plastic film mulching
$E_a$	bare soil evaporation	$E_{p,a}$	bare soil evaporation when soil moisture at field capacity

261

## 262 3. Results

### 263 3.1 Soil hydrophysical properties

264 An accurate measurement of soil hydraulic parameters is crucial for this inverse method and is helpful in explaining the  
 265 movement of soil water flow. A summary of the most important soil hydrophysical characteristics of the soils at 0–100-cm depth  
 266 (NT1 to NT6, and two other representative fields) in relation to their capacity for water storage is listed in Table 2. The textures





267 were largely loamy sandy in the plots NT1-NT6, in contrast to the sandy loam soil in an old oasis field with a long tillage history  
 268 (~100 years) and sandy soil in the desert with no tillage history (Table 2). Their bulk densities were generally between 1.4 and 1.5  
 269  $\text{g/cm}^3$ —slightly higher than that in the local desert land, but still lower than that in maize fields of the old oasis.  $\theta_s$ ,  $\theta_{fc}$  and  $\theta_w$   
 270 of the plots showed the same tendency of increasing soil hydrophysical properties (toward better water retention) as the bulk  
 271 densities (Table 2). However, those parameters of the soil profiles are very similar to each other, especially between the same soil  
 272 depths (horizontal) of the plots, suggesting that the different planting systems had similar influences on the soil hydrophysical  
 273 properties, at least at the scale of 10 years. The effects of different cropping systems on soil moisture release characteristics are  
 274 shown in Fig. 4. As expected, the relationship between soil water potential and volumetric water content across all data and treatment  
 275 combinations followed a curvilinear pattern, where the water potential increased exponentially as soil water content increased.

276 The large and varying values of saturated drainage velocity ( $K_s$ ) showed a great drainage potential in the coarse-textured soil  
 277 and an obvious heterogeneity in both horizontal and vertical profiles across the six plots (Table 2). Soil moisture characteristic  
 278 curves (SMC) in the six profiles are shown in Fig. 4, which indicates almost the same soil water content for all the plots, NT1-NT6,  
 279 under the same suction head; i.e., all the soil profiles were nearly saturated when the water potential reached the -0.01 bar and little  
 280 was available after the soil water potential dropped to the -15 bar. Two obvious inflection points were observed, at  $\theta \cong 0.08$  and  
 281  $0.3$ ,  $\psi \cong -0.32$  and  $-15.2$  bar in each of the soil moisture characteristic curves from NT1-NT6.  
 282 The slopes of the soil water potential-moisture, especially the parts between the inflection points of the six plots, were very close to  
 283 each other, and also similar to that of the desert soil, suggesting similarly poor water capacities of the sandy soils (Sławiński et al.,  
 284 2002). A very significant difference in water capacities was observed when comparing the SMC of NT1-NT6 with that of the old  
 285 oasis field, indicating that a considerably long period of time is still needed, for high soil water capacity to evolve, for these  
 286 experimental sites.

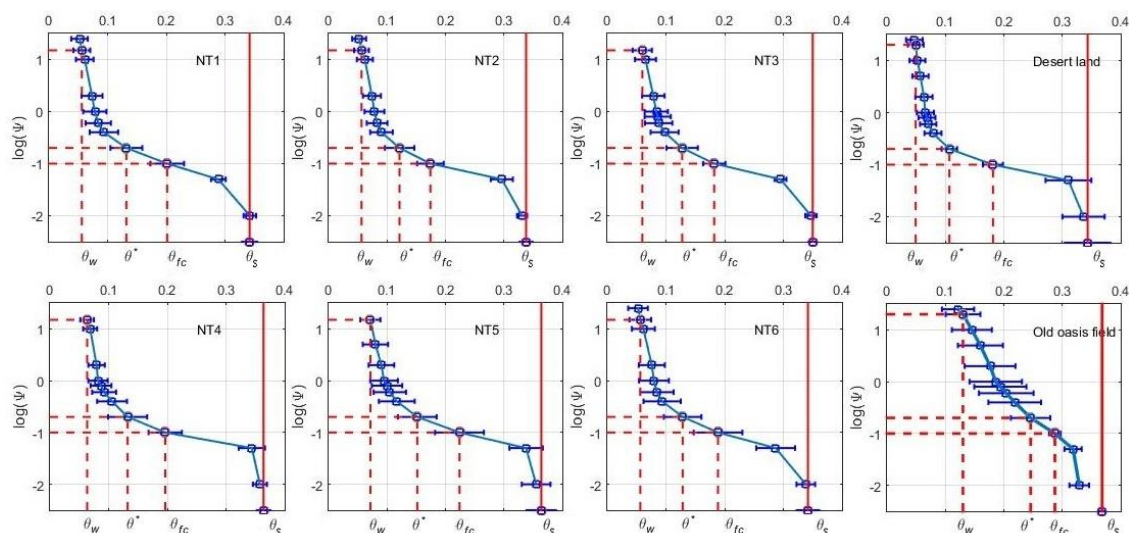
287

288 **Table 2.** Soil physical characteristics in the six experimental plots and two other selected plots around the study site

	NT1					NT2					NT3					NT4				
	$K_s$	$\rho_b$	$\theta_s$	$\theta_{fc}$	$\theta_w$	$K_s$	$\rho_b$	$\theta_s$	$\theta_{fc}$	$\theta_w$	$K_s$	$\rho_b$	$\theta_s$	$\theta_{fc}$	$\theta_w$	$K_s$	$\rho_b$	$\theta_s$	$\theta_{fc}$	$\theta_w$
20 cm	47.2	1.38	0.36	0.25	0.09	183	1.46	0.34	0.19	0.08	44.3	1.40	0.36	0.21	0.09	54.1	1.39	0.38	0.21	0.08
40 cm	46.8	1.55	0.33	0.21	0.06	82.1	1.55	0.32	0.15	0.05	259	1.54	0.34	0.18	0.06	266	1.50	0.36	0.17	0.06
60 cm	166	1.48	0.35	0.20	0.06	118	1.53	0.34	0.20	0.05	73.8	1.53	0.35	0.19	0.05	355	1.47	0.36	0.16	0.06
80 cm	61.0	1.45	0.33	0.17	0.05	164	1.48	0.35	0.18	0.05	1007	1.46	0.35	0.18	0.05	192	1.47	0.35	0.20	0.06
100 cm	273	1.46	0.34	0.18	0.05	99.7	1.49	0.34	0.15	0.05	46.1	1.44	0.35	0.16	0.05	80.0	1.40	0.37	0.23	0.06
$\bar{X}$	119	1.46	0.34	0.20	0.06	129	1.50	0.34	0.17	0.06	286	1.47	0.35	0.18	0.06	189	1.45	0.36	0.19	0.06
$SD$	99.6	0.06	0.01	0.03	0.02	42.8	0.04	0.01	0.02	0.01	413	0.06	0.01	0.02	0.02	126	0.05	0.01	0.03	0.01
	NT5					NT6					Maize field in old oasis					Local desert land				
	$K_s$	$\rho_b$	$\theta_s$	$\theta_{fc}$	$\theta_w$	$K_s$	$\rho_b$	$\theta_s$	$\theta_{fc}$	$\theta_w$	$K_s$	$\rho_b$	$\theta_s$	$\theta_{fc}$	$\theta_w$	$K_s$	$\rho_b$	$\theta_s$	$\theta_{fc}$	$\theta_w$
20 cm	121	1.42	0.37	0.24	0.09	89.6	1.50	0.32	0.25	0.09	28.8	1.61	0.38	0.29	0.11	42.5	1.46	0.36	0.16	0.05
40 cm	168	1.46	0.34	0.19	0.07	575	1.53	0.33	0.20	0.06	20.2	1.61	0.37	0.28	0.12	48.1	1.46	0.35	0.17	0.05
60 cm	41.3	1.39	0.40	0.29	0.09	66.5	1.45	0.37	0.18	0.05	37.4	1.56	0.38	0.28	0.10	30.9	1.44	0.39	0.20	0.07
80 cm	38.3	1.49	0.37	0.21	0.05	331	1.50	0.34	0.18	0.04	76.3	1.59	0.37	0.24	0.09	33.3	1.45	0.33	0.18	0.05
100 cm	671	1.47	0.34	0.19	0.06	18.6	1.47	0.35	0.14	0.04	47.5	1.58	0.40	0.29	0.12	26.9	1.43	0.28	0.17	0.03
$\bar{X}$	208	1.45	0.36	0.22	0.07	216	1.49	0.34	0.19	0.06	42	1.59	0.38	0.28	0.11	36	1.45	0.34	0.17	0.05
$SD$	265	0.04	0.02	0.04	0.02	234	0.03	0.02	0.04	0.02	22	0.02	0.01	0.02	0.01	9	0.01	0.04	0.02	0.01

289  $K_s$ : saturated water conductivity (cm/day);  $\rho_b$ : bulk density ( $\text{g/cm}^3$ );  $\theta_s$ : saturated water content (100%);  $\theta_{fc}$ : field capacity (100%) and  $\theta_w$ :  
 290 wilting point (100 %);  $\bar{X}$ : mean value of the five soil layers;  $SD$ : standard deviation of the five soil layers.

291



292

293 **Figure 4.** Soil moisture characteristic curve (SMC) of uniform soil profiles of the six experimental plots and two other representative fields. Soil  
 294 field capacity ( $\theta_{fc}$ ), wilting point ( $\theta_w$ ), and water stress point, i.e., point of incipient stomatal closure ( $\theta^*$ ) are empirically related to the  
 295 corresponding soil matric potentials (-0.1 bar for  $S_{fc}$ , -0.2 bar for  $\theta^*$  and -15 bar for  $S_w$ ); the blue horizontal line represents the error bar, and  
 296 the solid red line represents saturated water content ( $\theta_s$ ), which was obtained via the traditional soil drying method with 3 repetitions in each  
 297 layer; for soil water (matric) potential ( $\Psi$ ) take the absolute value, for example, -0.01 bar is equal to -2 on the Y axis.

### 298 3.2 Meteorological and irrigation data

299 The mean temperature of the growing season in 2016 was 27.12°C, or 3.12 degrees Celsius warmer than the long-term average  
 300 of the growing seasons in 2007-2016 (24.0°C), and the mean rainfall during the period was about 60.2 mm, or 47 percent less than  
 301 the long-term average of 115.4 mm (2005-2016), indicating that the weather was hotter and drier during the growing season in 2016  
 302 than in the previous ten years. Fig. 7 presents a summary of the amount of water applied over the entire growing season of 2016.  
 303 Irrigation applications began in mid-April and continued until late September, every 5 to 25 days, depending upon moisture content  
 304 and crop growth (Fig. 3). A total of 10 irrigation events were sequentially applied through furrow irrigation for the plot during the  
 305 entire growing season. Based on the in-situ observations of irrigation—i.e., the power consumption of the pumping irrigation well—  
 306 the estimated irrigation volumes of the six plots were averaged and tested against the observations at field scale.  
 307 The estimated average cumulative irrigation volume of the six plots during the entire growing season was 831.6 mm (i.e., 1187, 760,  
 308 652, 840, 683, and 867 mm for NT1 to NT6, respectively), which compares well with the actual average irrigation volume (868.8  
 309 mm) determined through power consumption, suggesting that the calculated irrigation agrees closely with the real values from the  
 310 farm fields when accurate irrigation and rainfall data are available. A difference of 4.5% in the irrigation amount was observed  
 311 between the real values and the estimated values over the entire growing season of 2016, indicating a high reliability of the water  
 312 balance method used in the *SWBCs* estimation.

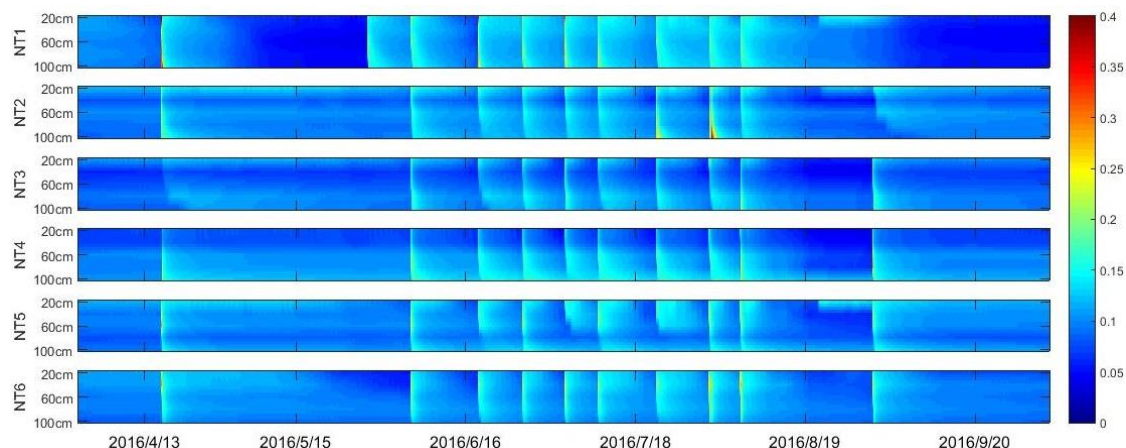
### 313 3.3 Soil moisture dynamics (SMDs)

314 Because the inverse method proposed by Zuo et al. (2002) and Guderle and Hildebrandt (2015) had never been applied  
 315 throughout an entire growing season for farmland, checking the soil water dynamic of the entire growing season can help us verify  
 316 the boundary setting and affirm the assumption about the irrigation estimation used. Fig. 2a shows an example of the soil water  
 317 content responses at various depths of NT6 during and after the irrigation event of 107.1 mm on DOY 154 (2016). TDR  
 318 measurements exhibited a sharp increase when irrigation began and then decreased rapidly as it was turned off, due to the poor  
 319 water-holding capacity of the sandy soil. The increase in water content occurred layer by layer from the upper horizons, suggesting  
 320 limited influence from potential preferential flow (Liu and Lin, 2015), while the rapid moistening of the deep horizons could imply  
 321 the existence of water loss by drainage. The greatest rate decrease in water content was observed in the top 20 cm of soil. During  
 322 the 12 h after irrigation, the water content at the top sensor decreased from 21.9% to 14.2%. For the same interval of time the water



323 contents in the 40-, 60-, 80- and 100-cm depths of soil decreased from 25.4%, 19.8%, 18.5% and 14.2% to 15.7%, 14.3%, 15.4%  
324 and 12.8%, respectively. After irrigation ended, water continued to move down the soil profile; and thus the top part of the profile  
325 was continuously losing water to the soil below it. The lower soil horizons were leaching water into the horizon below but at the  
326 same time were receiving water that had drained from the horizon immediately above, resulting in lower rates of decrease in water  
327 content for these layers than for those at the top horizon (20 cm) (Fares and Alva, 2000). Very similar patterns of changes in water  
328 content were observed through the six different soil profiles.

329 The average field capacity value ( $\theta_{fc}$ ) of NT1-6 determined from laboratory measurement of soil water release curves was  
330 19.2% (i.e., 20%, 17%, 18%, 19%, 22% and 19% for NT1-6 respectively). Twenty-four hours after the end of irrigation (June 3,  
331 2016), the soil moisture values for the all the measured horizons (20-100 cm depth) of NT1-6 ranged between 8.9% and 16.9%  
332 (13.7-15.7%, 13.7-15.1%, 8.9-14.5%, 9.6-16.9%, 11.7-15.3% and 12.3-14.2% for NT1-6 respectively), lower than the field capacity  
333 (Figs. 2 and 5), suggesting that the rapid drainage of water away from the root zone soil (0-100 cm) was terminated during the  
334 period, as expected. In the mornings of the subsequent days, the decrease in soil moisture again sped up as the evaporative demand  
335 of the atmosphere gradually increased. In the absence of any irrigation during the subsequent nights, a slow-down in the decrease  
336 or even a very light increase, in the soil moisture content was observed in the top soil layer (Fig 2). According to the data, there was  
337 also no obvious response of soil moisture regimes to precipitation, indicating a very limited contribution of rainfall to the soil water  
338 storage compared with irrigation. In fact, more than 90% of the rainfall events in this region are less than 5 mm (Fig. 3), and canopy  
339 interception (about 2-5 mm) may have hampered any effective infiltration from those insufficient precipitation events.  
340



341  
342 **Figure 5.** Spatial and temporal variations of soil water content with a time resolution of ten minutes. The color bar on the right side represents  
343 volumetric soil water content. Time period was from Apr. 1 to Oct. 1, 2016. Irrigation events for NT2-6 occurred on 4/16, 6/2, 6/15, 6/23, 7/1, 7/7,  
344 7/18, 7/28, 8/3, and 8/28. NT1 had one more irrigation event on 5/25 and one less on 8/28.

### 345 3.4 Soil water budget components (SWBCs)

346 The estimated soil water budget components, including total irrigation, deep percolation, and *ET*, at the six different plots  
347 during the growing season of 2016 are summarized in Table 3 and Fig. 7. Evapotranspiration and deep percolation dominated the  
348 fields' relatively simple soil water budgets during the study period. A clear trend in seasonal variation of the water budget  
349 components can be observed at the site (Fig. 7). The corresponding *ET* values were very similar for all the plots. Three different  
350 stages of *ET* could be discriminated throughout the 2016 growing season: *ET* rate was very low at the initial stage (i.e., the first 50  
351 days of the growing season), and increased gradually as vegetation coverage became greater with crop development, before reaching  
352 maximal values at the mid-season stage. After that, *ET* decreased gradually until harvest time. The estimated daily *ET* values ranged  
353 largely between 0.2 and 12 mm d<sup>-1</sup>, with an average of 3 mm d<sup>-1</sup>. No significant differences were detected in the daily *ET* when  
354 Duncan's multiple range test was applied at the 5% level to compare among the six experimental plots ( $P > 0.75$ ). A relatively large  
355 difference was observed between selected plots in this study, i.e., significantly higher cumulative irrigation volume was found at  
356 NT1. The excess of water in the soil produced an important deep percolation, which became greater with the increase in the irrigation



357 quota. Among the plots, 45-79% of the input irrigation water was consumed by way of ET (i.e. for plant growth), while the change  
 358 in soil water storage before and after the growing season was quite small. It is clear that although there was a high correlation  
 359 between the volume of irrigation and that of drained water, the superfluous irrigation amount had limited influence on the  
 360 accumulated ET during the growing season.

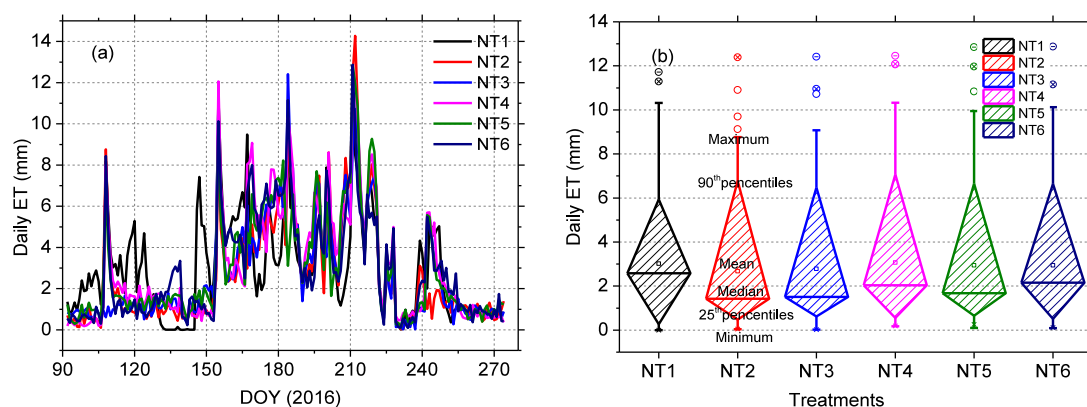
361  
 362

**Table 3.** Estimated evapotranspiration and other major soil water budget components during the growing season of 2016

Cumulative SWBCs	NT1	NT2	NT3	NT4	NT5	NT6
Irrigation	1186.5	760.1	652.2	840.4	683.2	867.3
Drainage	651.8	288.3	170.7	340.1	212.4	364.7
ET	534.6	489.1	508.8	561.9	539.2	538.1
Storage diff.*	-52.7	0.17	3.6	2.2	5.44	-11.64

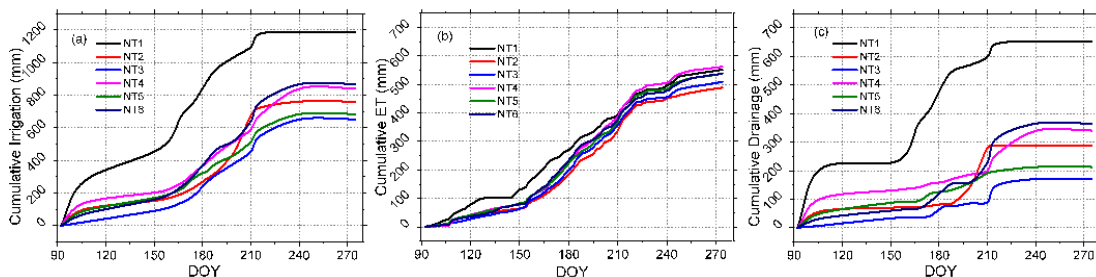
\* Storage differences represent the difference in soil water storage before and after the growing season.

363  
 364  
 365



366  
 367  
 368  
 369  
 370

**Figure 6.** Daily ET during the growing season of 2016 as determined from the inverse Richards method: a) time series of estimated daily ET; b) box-and-whisker diagrams showing the minimum, median, 25th percentile, 75th percentile, and maximum daily ET. No significant differences were detected when Duncan's multiple range test was applied at the 5% level to compare values among the plots.



371  
 372  
 373  
 374

**Figure 7.** Estimated water components of the plots during the growing season of 2016: a) cumulative irrigation, b) cumulative ET, c) cumulative drainage

## 375 4. Discussion

### 376 4.1 Estimated ET

377 Cumulative ET values calculated from inverse Richards methods ranged between 489.1 and 561.9 mm for the different  
 378 treatments in 2016. The values of ET obtained from the current study are well within the range of published ET values at the nearby  
 379 sites (406-778 mm), and are consistent with the averages from other studies (~585.5mm) also done in this region, including Zhao  
 380 and Ji (2010); Rong (2012); Yang et al. (2015); You et al. (2015); Zhao et al. (2015), etc. for maize fields similar to the ones present  
 381 at the study site (Table 4). Compared with the methods used in the literatures listed in Table 4, the soil-moisture data-based method  
 382 used in this study is more reliable because it produced a better fit between the numerical solution (soil water profile calculated by  
 383 the inverse Richards equation) and the measured values of soil moisture content (soil water profile measured by TDR), even with



384 vertical flow accounted for (Guderle and Hildebrandt, 2015). The narrow range of cumulative ET (489.1-561.9 mm) observed in  
 385 2016 can be attributed to the similar sandy soil texture and mesic moisture regimes caused by frequent irrigation (Figs. 4 and 5),  
 386 which in turn suggested that for the unmulched alfalfa and mulched maize, both cropping systems and agronomic manipulation had  
 387 limited influence on the accumulated ET during the growing season (Srivastava et al., 2017). This result is well supported by the  
 388 evidence reported by early investigators, that the ET differences in different cropping systems are quite small for coarse-textured  
 389 soils compared with the large differences in the amount of irrigation water (Jalota and Arora, 2002; Ji et al., 2007), and that ET is  
 390 strictly a function of ambient atmospheric conditions under normal or wet conditions (Rahgozar et al., 2012).

391 The observed seasonal trend of ET corresponded well to the irrigation frequency and crop water consumption characteristics  
 392 of the growth stage (Fig. 7), and similar patterns in the ET processes have also been reported by many other researches conducted  
 393 in this region (Zhao et al., 2015; Zhao et al., 2010). Although we also noticed that the cumulative ET of NT1 was relatively higher  
 394 than those of the other plots at the beginning of the growing season, this phenomenon can be largely attributed to the plastic film  
 395 mulching at the other five plots. In the early growing season (seeding to emergence), soil evaporation (E) is the major part of ET  
 396 (Zhao et al., 2015), and the plastic film mulching applied to NT2 to NT6 was able to significantly retain the soil moisture and thus  
 397 decrease soil evaporation (Jia et al., 2006). However, the differences in the cumulative ET, between NT1 and the other plots, were  
 398 quite small after the mid-growing season, most likely because with the plant canopy development, crop transpiration became the  
 399 major portion of ET, and the influence of plastic film on ET diminished (Zhang et al., 2017; Qin et al., 2014; Jia et al., 2006). Another  
 400 influence that may have decreased the evapotranspiration at NT1 after the mid-growing season is cutting. Cutting alfalfa lowers the  
 401 leaf area index (LAI) and drastically changes the effective diffusive resistance, consequently lowering the daily ET rate of alfalfa at  
 402 NT1, although for a short time after cutting, evaporation from the soil surface may compensate for the decrease in transpiration  
 403 (Dong et al., 2003; Su et al., 2010).

404

405

**Table 4.** Reported ET of oasis maize field in the middle Heihe River Basin (HRB)

ET (mm)	Growing period	Year	Soil type	Irrigation	Rainfall	Methods	Paper
651.6	Apr.11-Sep.18	2001	---	690	84.4	Water balance methods	(Peixi et al., 2002)
513.2	Apr.16-Sep.22	2005	Light loam	360	153.5	Bowen ratio method	(Jinkui et al., 2007)
486.2	Apr.16-Sep.22	2005	Light loam	360	153.5	Reference ET-crop coefficient method	(Jinkui et al., 2007)
777.75	Apr.21-Sep.15	2007	Sandy loam	1194	102.1	Bowen ratio method	(Zhao et al., 2010)
693.13	Apr.21-Sep.15	2007	Sandy loam	1194	102.1	Penman	(Zhao et al., 2010)
618.34	Apr.21-Sep.15	2007	Sandy loam	1194	102.1	Penman-Monteith	(Zhao et al., 2010)
615.67	Apr.21-Sep.15	2007	Sandy loam	1194	102.1	Water balance method	(Zhao et al., 2010)
560.31	Apr.21-Sep.15	2007	Sandy loam	1194	102.1	Priestley-Taylor	(Zhao et al., 2010)
552.07	Apr.21-Sep.15	2007	Sandy loam	1194	102.1	Hargreaves method	(Zhao et al., 2010)
671.2	Apr.10-Sep.20	2009	Sandy loam	797	97.7	FAO-56-PM and dual crop coefficient method	(Zhao and Ji, 2010)
640	Apr.10-Sep.20	2009	---	797	97.7	Shuttleworth-Wallace dual-source model	(Zhao et al., 2015)
570—607	Apr.22-Sep.23	2010	Loamy sand	990-1103	75	Field experiments	(Rong, 2012)
405.5	Apr.20-Sep.22	2012	Clay loam	553	95.9	Water balance and isotope methods	(Yang et al., 2015)
450.7	Apr.20-Sep.22	2012	---	430	104.9	Eddy covariance system	(You et al., 2015)
554.0	Apr.20-Sep.22	2012	---	430	104.9	Penman	(You et al., 2015)
489-562	Apr.10-Sep.20	2016	Sandy soil	652-867	60.2	Inverse method	This paper

406

#### 407 4.2 Other estimated SWBCs in this study

408 The irrigation volume of maize (NT2 to NT6) within our plots ranged between 652.2 and 867.3 mm, with an average value of  
 409 760.6 mm, which is well comparable to the range of average maize field irrigation volume in this region, i.e., a range between 604.8  
 410 and 811.4 mm reported in the Statistical Yearbook of Zhangye City for the period of 1995 to 2017 (see <http://www.zhangye.gov.cn>).  
 411 When compared to the other treatments of plastic film mulching, significantly higher amounts of the applied irrigation (1186.5 mm)  
 412 were found in NT1, which could be attributed to the larger percentage of infiltrating surface area and the relatively longer irrigation  
 413 duration caused by rougher surface of the ground without plastic film mulching. According to Yang et al. (2018a), plastic film mulch  
 414 has been widely used to increase the productivity of crops in arid or semiarid regions of China. The logic behind this approach is  
 415 that plastic film mulch improves the soil physical properties, such as the soil water content and temperature in the top soil layers,  
 416 and thus leads to increased plant growth and yield (N. Mbah et al., 2010). Our results suggested that plastic film mulching can  
 417 equally reduce irrigation duration and applied water depth by lowering surface roughness and thus the friction coefficient of the  
 418 ground. Similar results were also reported by earlier investigators (Zhang et al., 2017; Jia et al., 2006; Qin et al., 2014).  
 419 A less extreme but still significant difference can be found in the irrigation volumes (~652.2 to 867.3 mm) over the other five plots  
 420 with plastic film mulching (NT2-6). This may be associated with the inconsistent durations caused by uneven irrigation applications,





421 randomly rough soil surfaces, and mutation of the infiltration rate (i.e.,  $K_s$ ) across the plots (Table 2). Uneven irrigation may be  
422 further attributed to the uneven fields and ditches, which may lead to the application of much more water than required for  
423 evapotranspiration, in some places (Babcock and Blackmer, 1992). Soil surface texture has a direct effect on soil water and complex  
424 interactions with other environmental factors (Yong et al., 2014). The hydraulic behavior and the rate of traditional surface irrigation  
425 is eventually influenced by the inflow and duration of each irrigation (Ascough and Kiker, 2002). Although only slight differences  
426 exist among the retention curves (Fig. 4), the differences in saturation water conductivity ( $K_s$ ) can be substantial (varying between  
427 119 cm/day at NT1 and 286 cm/day at NT3), indicating that a slight difference in hydrophysical properties of soil profiles could be  
428 amplified to generate wildly varying infiltration behavior, especially during saturated or near-saturated stages under actual irrigation  
429 conditions (Ojha et al., 2017).

430 In desert oasis farmland, the water cycle is primarily driven by evapotranspiration demand under the influence of irrigation,  
431 and soil water percolation may occur when too much water is applied to the root zone. Estimated deep drainage rates were observed,  
432 ranging from 170.7 mm (NT3) to 651.8 mm (NT1), amounting to about 26.2% and 54.9% of the total irrigation of the two plots,  
433 respectively. Drainage within the mulched maize fields ranged from 170.7 mm to 364.7 mm, which are in good agreement with  
434 other results from the same region, i.e., 255 mm through isotopes obtained by Yang et al. (2015), and 339.5 mm through the Hydrus-  
435 1D model by Dong-Sheng et al. (2015). Compared with the theoretical deep drainage determined by water balance techniques (Rice  
436 et al., 1986), an error of -2.6 to 43.1 mm, or 0.2 % to 17.6%, was obtained for the cumulative deep drainage (Table 3), indicating  
437 the reliability of the method used to estimate deep drainage in this study. The data expressed in Fig. 2 also explain how easily an  
438 excess of water, and therefore deep drainage, can occur in these soils. Indeed, the deep drainage was directly proportional to the  
439 amount of irrigation applied during any particular period (Fig. 7, Table 3). This phenomenon is easy to understand because for a  
440 given amount of irrigation, the likelihood of a drainage event and its average size both increased naturally with the irrigation amount  
441 (Fig. 7) (Keller, 2005). It is obvious that drainage should be an essential part of irrigation design and management. According to our  
442 results, an average of 40.6% of input water was consumed by deep leakage across the six plots; this is unproductive and could even  
443 cause nutrient loss and groundwater pollution at field scales (Fares and Alva, 2000), suggesting there is a huge potential for  
444 increasing irrigation water-use efficiencies and reducing irrigation water requirements in this region.

#### 445 4.3 Effects of different cropping systems and tillage periods on soil hydrophysical properties

446 In this desert oasis with constant expansion, most of the fields belong to smallholder farmers, who usually follow different  
447 tillage periods and special cropping patterns, resulting in a heterogeneity of soil hydrophysical properties (Salem et al., 2015; Ács,  
448 2005; Abu and Abubakar, 2013). For the soil-moisture data-based method proposed in this paper, the spatial heterogeneity of the soil  
449 hydrophysical properties—which can be characterized by hydrophysical functions (soil water retention curve and soil water  
450 conductivity) and/or hydrophysical parameters ( $\rho_b$ ,  $\theta_s$ ,  $\theta_{fc}$  and  $\theta_w$ ) (Ács, 2005)—may restrict its applicability to a large  
451 agricultural area. Therefore, evaluating to what extent the different cropping systems and agronomic manipulations affect the soil  
452 hydrophysical properties is important, in order to reduce unnecessary repetitive measurements of soil hydrophysical information at  
453 both spatial and temporal scales, and thus improve the application efficiency of our method. Long-term cropping can increase annual  
454 water productivity by improving soil hydrophysical properties and reducing unproductive water losses (Caviglia et al., 2013). Crop  
455 root systems, for example, may create heterogeneity in soil properties through mechanical actions and the active release of chemicals  
456 (Hirobe et al., 2001; Read et al., 2003); and, along with similar feedbacks between long-term planted crops and the soil environment,  
457 may change water flow and soil hydraulic characteristics, and thus affect local water balances (Baldocchi et al., 2004; Sérén et al.,  
458 2012). Although it is difficult to quantify the consequences of plant-soil feedbacks on the hydrologic cycle of farmland, because of  
459 the lack of an accurate simulation model (Jalota and Arora, 2002), our results indicated that the tillage and planting of past decades  
460 have significantly increased the soil's water-holding ability (i.e., higher values of  $\rho_b$ ,  $\theta_s$ ,  $\theta_{fc}$  and  $\theta_w$  compared with the sandy  
461 land). The magnitude of increase in most of the parameters, except  $K_s$  in soil vertical profiles, was independent of the treatments  
462 applied across the six selected plots, which also suggests that different cropping systems and agronomic manipulation have limited  
463 effects on differing soil physical characteristics in sandy soil, at least at a decade scale, and this agrees well with the reports from  
464 Katsvairo et al. (2002). However, we argue that significant differences in soil hydrophysical properties among the plots may occur  
465 if the treatments are conducted over longer periods of time, i.e., ~100 years or more. In summary, the relatively slow process of soil  
466 evolution with tillage operations, and the limited influence of different cropping systems on soil hydrophysical properties at a 10-



467 year scale, indicate a good stability and representativeness of the measured soil hydrophysical data and thus a good application  
468 prospect for applying the soil-moisture data-based method in practice.

#### 469 **4.4 Potential for *SWBC* estimation by using soil moisture measurements**

470 The best estimates of *SWBCs* should be based on models of soil water, because in most cases direct measurements are not  
471 available (Campbell and Diaz, 1988). Many studies including modeling work have been conducted in this region during the past  
472 decades (Table 4). Since there has been a lack of accurate parameters to assess the heterogeneity and complexity involved in  
473 modeling (Allen et al., 2011;Suleiman and Hoogenboom, 2007;Wang and Dickinson, 2012;Ibrom et al., 2007), however, most of  
474 these were rough approximations based on meteorological methods and water balance equations (Rong, 2012;Jiang et al., 2016;Yang  
475 et al., 2015;Wu et al., 2015;Ji et al., 2007). Yet soil-moisture data-based methods have been considered one of the most promising  
476 ways to directly determine ET and other *SWBCs* (Guderle and Hildebrandt, 2015;Li et al., 2002), and many possible options,  
477 including single- or multi-step, and single- or multi-layer water balance methods, have been proposed and tested with synthetic time  
478 series of water content (Guderle and Hildebrandt, 2015). Our results suggest that a combination of a soil water balance method and  
479 the inverse method could be a good candidate for *SWBC* estimation in this region, and can provide a reliable solution, especially in  
480 regards to estimating ET, root water uptake, and water vertical flow, and do not require any prior information of root distribution  
481 parameters, and they can be applicable under both wet and dry weather conditions (Guderle and Hildebrandt, 2015).

482 Information on *SWBCs* is crucial for irrigation planning at both the field and regional scale (Jalota and Arora, 2002). Early  
483 researches suggested that decreasing the irrigation amount and increasing the irrigation frequency is the best choice for saving water  
484 and improving water use efficiency in the middle HRB (Rong, 2012;Jiang et al., 2016;Yang et al., 2015;Wu et al., 2015;Ji et al.,  
485 2007). This scenario can be achieved not only by adopting proper modern irrigation systems but also by integrating new technologies  
486 into the effective planning of irrigation schedules, so that plants can be supplied with optimal water volume and minimum water  
487 loss. Soil water budget models help in translating irrigation amounts in different time periods to evapotranspiration (ET), which has  
488 significance from the standpoint of crop yield (Jalota and Arora, 2002). Our results show that superfluous irrigation has no effect on  
489 increasing ET, because of the poor water-holding capacity of the sandy soil in this region, and thus irrigation application should not  
490 exceed a specific threshold (i.e., root zone depletion, ~527 mm for maize) to avoid deep percolation, which has a negative effect,  
491 increasing irrigation costs (Zotarelli et al., 2016). However, water deficits in crops and the resulting water stress on plants also  
492 influences crop evapotranspiration and crop yield (Kallitsari et al., 2011). Thus, a soil moisture measurement method based on  
493 *SWBC* estimation makes it possible to quantify water budget components for different time periods, and has great potential for  
494 identifying appropriate irrigation amounts and frequencies. As the price of commercial TDR systems has become affordable  
495 (Quinones and Ruelle, 2001), it is more and more frequently used for soil water content measurements in desert oases, and thus a  
496 soil-moisture data-based method has great potential in irrigation management optimization and in moving toward sustainable water  
497 resources management, even under traditional surface irrigation conditions (Tawara *et al.*, 2015).

#### 498 **4.5 Uncertainty analysis**

499 Uncertainty is inevitable, in any soil water budget components estimate. As summarized by Zuo et al. (2002) and (Guderle and  
500 Hildebrandt, 2015), the accuracy and convergence of estimated evapotranspiration and slow drainage using this inverse approach  
501 are dependent on several factors, including the accuracy of soil hydraulic parameters and input soil moisture data, the time intervals  
502 of soil water content measurements, the spatial interval of the measured data along the depth, the setting of simulation depth and  
503 the boundary conditions. For a soil-moisture data-based method, the estimated results are only as good as their input data, i.e., the  
504 accuracy, the precision and the resolution (Guderle and Hildebrandt, 2013;Guderle and Hildebrandt, 2015). In this study, every effort  
505 was made to eliminate the uncertainty caused by the quality of the input data: for example, all the sensors and cables were carefully  
506 buried according the operator's manual instructions; the soil-specific calibration of TDR was conducted in a well-designed  
507 laboratory calibration experiment, which results a good accuracy ( $\pm 2\%$ ) for TDR measurement in coarse-textured soil; and the  
508 high-resolution moisture data (taken at 10-minute intervals) were hourly averaged to numerically filter out the noise and improve  
509 the calculation speed of the inverse model. Meanwhile, the simulation depth (0-110cm) is consistent with the root depth, and it can  
510 be well represented by 5 TDR probes with a spatial interval of 20 cm in sandy soil (Zhao et al., 2016). The boundary condition is  
511 also important for this inverse model (Liao et al., 2016); as mentioned in Section 2.3.3, we set the upper and lower boundaries as



512 close as possible to natural conditions. However, we did not set specific upper boundaries for inter-cropping treatments, i.e., no bare  
513 soil evaporation was considered in the inter-cropping maize-pea field, which may have slightly underestimated the ET of NT6, but  
514 within an acceptable range because the soil evaporation of NT6 was relatively small when compared with the total transpiration  
515 over a growing season. Moreover, the high amount of irrigation may have reduced the temperature of the soil profile, because  
516 irrigation is often accompanied by an increase in latent heat flux, and thus by an increase in evapotranspiration (Chen et al.,  
517 2018;Haddeland et al., 2006;Zou et al., 2017). Theoretically, a decrease in soil temperature may slightly increase the soil suction  
518 under the same moisture conditions (Bachmann et al., 2002), and hence variations in the soil temperature profile under different  
519 irrigation scenarios may have affected the accuracy of the inverse model by changing the soil water retention curves. However,  
520 irrigation-affected variations of soil profile temperature in this study were small (within 2°C), which is smaller than the daily  
521 variation of soil temperature (2 to 3°C), and thus its effect on soil water retention curves can be ignored for eco-hydrological  
522 researches (Bachmann et al., 2002;Gao and Shao, 2015). Even so, it is still an interesting and important research field deserving  
523 further investigation.

524 Aside from the uncertainties in estimating evapotranspiration and slow drainages, more limitations may exist in the estimation  
525 of irrigation amounts and rapid drainages following irrigation events. Both of these limitations were strongly dependent on the  
526 assumptions of Equation (2) and (3), specifically, the estimation of  $S_{max}$ . We checked all the irrigation events of NT1-NT6 during  
527 the entire 2016 growing season, and results showed an acceptable accuracy of the estimation of  $S_{max}$  (only two irrigation events  
528 in NT2 slightly underestimated the  $S_{max}$ : 1.86 and 10.3 mm, which accounted for 1.1% and 4.1% of total soil water storage,  
529 respectively). This phenomenon—deep percolation that began before irrigation ceased—may have been caused by long irrigation  
530 duration time and high  $K_s$  of surface soil at NT2, which is the major limitation when applying our method to other regions.  
531 Calculating the previously occurring leakage volume, for example, using the unsaturated hydraulic conductivity empirical equation,  
532 is one of the possible solutions that needs to be tested in future work. Installing TDR under the film-mulched ridges may also cause  
533 an underestimation of the soil moisture content during an irrigation event. We investigated the difference caused by the location of  
534 TDR by comparing the soil water dynamics of an unmulched flat plot (NT1, which was independent of TDR location) and film-  
535 mulched ridge plots (NT2-6, which were affected by TDR location) after irrigation, and found that the underestimation caused by  
536 the location of TDR was mainly significant in the top 30 cm of the soil layer. For example, during the 24 hours after the irrigation  
537 on June 2 (DOY 154-155, Fig. 2), in the top 30 cm of the soil layer, the maximum soil moisture value of NT1 was 0.378 while the  
538 maximum soil moisture value of other plots (NT2-6) ranged between 0.219 and 0.299; in other layers, the maximum soil moisture  
539 value of NT1 was well within the maximum soil moisture values of other plots at the same layer, i.e., 0.189, 0.191, 0.174, 0.164 for  
540 NT1 and 0.154-0.254, 0.153-0.277, 0.154-0.205, 0.148-0.181 for the other plots. The minimum soil moisture values were very close  
541 between NT1 and the other plots at the same layer (<0.04). Meanwhile, the variances between NT1 and the other plots were 0.006  
542 to 0.009 in the top 30 cm of the soil layer, and 0.001-0.004, 0.003-0.004, 0.001-0.003, 0.002-0.004 for the other layers, which  
543 showed a good consistency of soil dynamics in the 30- to 110-cm soil layers compared with the top 30 cm of the soil layers. These  
544 consistencies may be because by 1) the height of ridge shoulders in the experimental plots was relatively low (<3cm), and substantial  
545 infiltration could occur through the film holes made for maize growth; 2) lateral water transfers could be substantially enhanced  
546 during the period of irrigation because of the soil water potential differences between ridges and furrows. This judgment also can  
547 be supported by some researches conducted in similar environments, e.g., Zhang et al. (2016). Therefore, we argue here that the  
548 uncertainty that TDR location brings to the  $SWBC$  estimations in this study is acceptable. For now, given that the effect of plastic  
549 mulched furrow irrigation on soil water distribution remains elusive (Zhang et al., 2016;Abbasi et al., 2004), installing TDR in both  
550 the ridge and the furrow may be a better choice in future studies. Besides, both the heterogeneity of soil hydrophysical properties in  
551 sandy soils and the rough artificial irrigation process can bring uncertainties in the irrigation amount of any oasis cropland. However,  
552 the maximum irrigation rate of flood or furrow irrigation is mainly dependent on the  $K_s$  of the top soil layer, which is nearly  
553 homogeneous in such small experimental plots (6m×9m) because they have the same cropping systems and agronomic history  
554 (Table 2), and thus there is no significant infiltration difference within one small plot, and the installed soil moisture probes can well  
555 monitor the irrigation process of the entire plot.

556 Overall, we are confident about the estimation accuracy of ET, which is the most important parameter among all the  $SWBCs$ ,  
557 and the one the related researchers are most interested in, because of its direct relevance to crop yield, and because maximizing crop  
558 yield is the major objective of agricultural irrigation strategies (Liu et al., 2002;Zhang et al., 2004;Kang et al., 2002). The ET



559 estimation model in this study not only has great advantages in theory (for example, it does not require any root distribution  
560 information (Schneider et al., 2010;Guderle and Hildebrandt, 2015)), but at the same time it also considers the hysteresis effect,  
561 unlike other common models (Li et al., 2002;Guderle and Hildebrandt, 2015), while also providing a reliable and high-resolution  
562 solution because its results are well within the range of published ET values at nearby sites. Other *SWBC* estimations such as  
563 irrigation, also had an acceptable accuracy, even though they were estimated by a relatively simple method, because the results show  
564 a good consistency with the observations (actual irrigation calculated from the power consumption) at the field scale and with the  
565 average irrigation amounts in other maize fields in the same region at close to the same time.

## 566 5. Conclusions

567 A database of soil moisture measurements taken in 2016 from six experimental fields (which were originally designed to test  
568 the accumulative impacts of different cropping systems and agronomic manipulations on soil-property evolution in the ecotone of  
569 desert and oasis) in the middle Heihe River Basin of China, was used to test the potential of a soil-moisture time series for estimating  
570 the *SWBCs*. We compared the hydrophysical properties of the soils in the plots, and then determined evapotranspiration and other  
571 *SWBCs* through a soil-moisture data-based method that combined both the soil water balance method and the inverse Richards  
572 equation, and the uncertainties of the employed methods were analyzed at the end of the experiment. Our results confirmed that (1)  
573 relatively reasonable estimations of the *SWBCs* in a desert oasis environment can be derived by using soil moisture measurements.  
574 Although uncertainties exist, our method, which balanced simplicity and accuracy, can provide a reliable solution, especially in  
575 regards to estimating ET, for coarse-textured sandy soils; (2) although the tillage and planting of the past decade have significantly  
576 increased the soil water-holding ability, the magnitude of increase in most of the soil hydrophysical parameters was independent of  
577 the different treatments applied across the plots during a 10-year period, resulting in a good prospect for applying our method among  
578 different fields; (3) the estimated results of the *SWBCs* will provide a valuable reference for optimizing irrigation strategies at the  
579 field scale, but it is still a long way from use on large areas of agricultural land, because of the soil heterogeneity at the regional  
580 scale and the small volume that a TDR probe can monitor.

581

## 582 Acknowledgements

583 This research was jointly supported by the National Natural Science Foundation of China (No. 41630861), the Youth  
584 Innovation Promotion Association of Chinese Academy of Sciences, and the West Light Foundation of Chinese Academy of  
585 Sciences (No. 29Y929621). We would like to thank Dr. Yang Yu for his constructive suggestions on completing this work. Special  
586 thanks also go to editor Fuqiang Tian, Dr. Jun Niu, Dr. Yanjun Shen, Dr. L. Brocca, and the other anonymous reviewers, whose  
587 perceptive criticisms, comments and suggestions helped us improve the quality of the manuscript.

588

## 589 References

- 590 Abbasi, F., Feyen, J., and Genuchten, M. T. V.: Two-dimensional simulation of water flow and solute transport below furrows: model calibration  
591 and validation, *Journal of Hydrology*, 290, 63-79, <https://doi.org/10.1016/j.jhydrol.2003.11.028>, 2004.
- 592 Abu, S. T., and Abubakar, I. U.: Evaluating the effects of tillage techniques on soil hydro-physical properties in Guinea Savanna of Nigeria, *Soil  
593 and Tillage Research*, 126, 159-168, <https://doi.org/10.1016/j.still.2012.09.003>, 2013.
- 594 Ács, F.: On Transpiration and Soil Moisture Content Sensitivity to Soil Hydrophysical Data, *Boundary-Layer Meteorology*, 115, 473-497,  
595 <https://doi.org/10.1007/s10546-004-5937-8>, 2005.
- 596 Allen, R., Irmak, A., Trezza, R., Hendrickx, J. M. H., Bastiaanssen, W., and Kjaersgaard, J.: Satellite-based ET estimation in agriculture using  
597 SEBAL and METRIC, *Hydrological Processes*, 25, 4011-4027, <https://doi.org/10.1002/hyp.8408>, 2011.
- 598 Ascough, G. W., and Kiker, G. A.: The effect of irrigation uniformity on irrigation water requirements, *Water SA*, 28, 235-241,  
599 <https://doi.org/10.4314/wsa.v28i2.4890>, 2002.
- 600 Babcock, B. A., and Blackmer, A. M.: The Value of Reducing Temporal Input Nonuniformities, *Journal of Agricultural and Resource Economics*,  
601 17, 335-347, 1992.
- 602 Bachmann, J., Horton, R., Grant, S. A., and Van der Ploeg, R.: Temperature dependence of water retention curves for wetttable and water-repellent  
603 soils, *Soil Science Society of America Journal*, 66, 44-52, <https://doi.org/10.2136/sssaj2002.4400>, 2002.



- 604 Baldocchi, D. D., Xu, L., and Kiang, N.: How plant functional-type, weather, seasonal drought, and soil physical properties alter water and energy  
605 fluxes of an oak-grass savanna and an annual grassland, *Agricultural and Forest Meteorology*, 123, 13-39,  
606 <https://doi.org/10.1016/j.agrformet.2003.11.006>, 2004.
- 607 Bautista, E., and Wallender, W. W.: Reliability of Optimized Furrow-Infiltration Parameters, *Journal of Irrigation and Drainage Engineering*, 119,  
608 784-800, [https://doi.org/10.1061/\(ASCE\)0733-9437\(1993\)119:5\(784\)](https://doi.org/10.1061/(ASCE)0733-9437(1993)119:5(784)) 1993.
- 609 Bethune, M. G., Selle, B., and Wang, Q. J.: Understanding and predicting deep percolation under surface irrigation, *Water Resources Research*,  
610 44, 681-687, <https://doi.org/10.1029/2007WR006380>, 2008.
- 611 Bourazanis, G., Rizos, S., and Kerkides, P.: Soil water balance in the presence of a shallow water table, in: *Proceedings of 9th World Congress*,  
612 *Istanbul, Turkey, June 2015*, 119-142, 2015.
- 613 Campbell, G. S., and Diaz, R. (Eds.): Simplified soil-water balance models to predict crop transpiration, in: *Drought Research Priorities for the*  
614 *Dryland Tropics*, edited by: Bidinger, F.R., and Johansen, C., ICRISAT (International Crops Research Institute for the Semi-Arid Tropics),  
615 Patancheru, India, 15-26, 1988.
- 616 Caviglia, O. P., Sadras, V. O., and Andrade, F. H.: Modelling long-term effects of cropping intensification reveals increased water and radiation  
617 productivity in the South-eastern Pampas, *Field Crops Research*, 149, 300-311, <https://doi.org/10.1016/j.fcr.2013.05.003>, 2013.
- 618 Celia, M. A., Bouloutas, E. T., and Zarba, R. L.: A general mass-conservative numerical solution for the unsaturated flow equation, *Water Resources*  
619 *Research*, 26, 1483-1496, <https://doi.org/10.1029/WR026i007p01483>, 1990.
- 620 Chen, R., Kang, E., Ji, X., Yang, J., and Wang, J.: An hourly solar radiation model under actual weather and terrain conditions: A case study in  
621 Heihe river basin, *Energy*, 32, 1148-1157, <https://doi.org/10.1016/j.energy.2006.07.006>, 2007.
- 622 Chen, Y., Niu, J., Kang, S., and Zhang, X.: Effects of irrigation on water and energy balances in the Heihe River basin using VIC model under  
623 different irrigation scenarios, *Science of The Total Environment*, 645, 1183-1193, <https://doi.org/10.1016/j.scitotenv.2018.07.254>, 2018.
- 624 Costa-Cabral, M. C., Richey, J. E., Goteti, G., Lettenmaier, D. P., Feldkotter, C., and Snidvongs, A.: Landscape structure and use, climate, and  
625 water movement in the Mekong River basin, *Hydrological Processes* 22, 1731-1746, <https://doi.org/10.1002/hyp.6740>, 2008.
- 626 Dejen, Z. A.: Hydraulic and operational performance of irrigation schemes in view of water saving and sustainability: sugar estates and community  
627 managed schemes In Ethiopia, CRC Press/Balkema, Leiden, The Netherlands, 2015.
- 628 Deng, X. P., Shan, L., Zhang, H., and Turner, N. C.: Improving agricultural water use efficiency in arid and semiarid areas of China, *Agricultural*  
629 *Water Management*, 80, 23-40, <https://doi.org/10.1016/j.agwat.2005.07.021>, 2006.
- 630 Dolman, A., and De Jeu, R.: Evaporation in focus, *Nature Geoscience*, 3, 296-296, <https://doi.org/10.1038/ngeo849>, 2010.
- 631 Dong-Sheng, L. I., Xi-Bin, J. I., and Zhao, L. W.: Simulation of Seed Corn Farmland Soil Moisture Migration Regularity in the Midstream of the  
632 Heihe River Basin, *Arid Zone Research*, 3, 467-475, <https://doi.org/10.13866/j.azr.2015.03.08>, 2015.
- 633 Dong, X., Hong, X. U., and Ji-Cun, P. U.: Extraction of Remote Sensing Information of Spring Crops Under Support of GPS and GIS in Yunnan  
634 Province, *Agricultural Meteorology*, 24, 35-37, <https://doi.org/10.3969/j.issn.1000-6362.2003.04.011>, 2003.
- 635 Fares, A., and Alva, A. K.: Evaluation of capacitance probes for optimal irrigation of citrus through soil moisture monitoring in an entisol profile,  
636 *Irrigation Science*, 19, 57-64, <https://doi.org/10.1007/s002710050001>, 2000.
- 637 Folhes, M. T., Rennó, C. D., and Soares, J. V.: Remote sensing for irrigation water management in the semi-arid Northeast of Brazil, *Agricultural*  
638 *Water Management*, 96, 1398-1408, <https://doi.org/10.1016/j.agwat.2009.04.021>, 2009.
- 639 Fu, B., Li, S., Yu, X., Ping, Y., Yu, G., Feng, R., and Zhuang, X.: Chinese ecosystem research network: Progress and perspectives, *Ecological*  
640 *Complexity*, 7, 225-233, <https://doi.org/10.1016/j.ecocom.2010.02.007>, 2010.
- 641 Gao, H., and Shao, M.: Effects of temperature changes on soil hydraulic properties, *Soil and Tillage Research*, 153, 145-154,  
642 <https://doi.org/10.1016/j.still.2015.05.003>, 2015.
- 643 Gardner, W., and Mayhugh, M.: Solutions and Tests of the Diffusion Equation for the Movement of Water in Soil, *Soil Science Society of America*  
644 *Journal*, 22, 197-201, <https://doi.org/10.2136/sssaj1958.03615995002200030003x>, 1958.
- 645 Grayson, R. B., Blöschl, G., Willgoose, G. R., and McMahon, T. A.: Observed spatial organization of soil moisture and its relation to terrain indices,  
646 *Water Resources Research*, 35, 797-810, <https://doi.org/10.1029/1998wr900065>, 1999.
- 647 Guderle, M., and Hildebrandt, A.: Using measured soil water contents to extract information on summer evapotranspiration and root water uptake  
648 patterns, in: *EGU General Assembly Conference, Vienna, Austria, 7 April 2013*, 15, 2013
- 649 Guderle, M., and Hildebrandt, A.: Using measured soil water contents to estimate evapotranspiration and root water uptake profiles – a comparative  
650 study, *Hydrology and Earth System Sciences*, 19, 409-425, [10.5194/hess-19-409-2015](https://doi.org/10.5194/hess-19-409-2015), 2015.





- 651 Haddeland, I., Lettenmaier, D. P., and Skaugen, T.: Effects of irrigation on the water and energy balances of the Colorado and Mekong river basins,  
652 *Journal of Hydrology*, 324, 210-223, <https://doi.org/10.1016/j.jhydrol.2005.09.028>, 2006.
- 653 Hamblin, A. P.: The influence of soil structure on water movement, crop root growth, and water uptake, *Advances in Agronomy*, 38, 95-158,  
654 [https://doi.org/10.1016/S0065-2113\(08\)60674-4](https://doi.org/10.1016/S0065-2113(08)60674-4), 1985.
- 655 Hanks, R. J., and Bowers, S. A.: Numerical Solution of the Moisture Flow Equation for Infiltration into Layered Soils<sup>1</sup>, *Soil Science Society of  
656 America Journal*, 26, 530, <https://doi.org/10.2136/sssaj1962.03615995002600060007x>, 1962.
- 657 Hirobe, M., Ohte, N., Karasawa, N., Zhang, G. S., Wang, L. H., and Yoshikawa, K.: Plant species effect on the spatial patterns of soil properties  
658 in the Mu-us desert ecosystem, Inner Mongolia, China, *Plant and Soil*, 234, 195-205, <https://doi.org/10.1023/A:1017943030924>, 2001.
- 659 Hu, K., Li, B., Chen, D., Zhang, Y., and Edis, R.: Simulation of nitrate leaching under irrigated maize on sandy soil in desert oasis in Inner  
660 Mongolia, China, *Agricultural Water Management*, 95, 1180-1188, <https://doi.org/10.1016/j.agwat.2008.05.001>, 2008.
- 661 Ibrom, A., Dellwik, E., Flyvbjerg, H., Jensen, N. O., and Pilegaard, K.: Strong low-pass filtering effects on water vapour flux measurements with  
662 closed-path eddy correlation systems, *Agricultural and Forest Meteorology*, 147, 140-156, <https://doi.org/10.1016/j.agrformet.2007.07.007>, 2007.
- 663 Jalota, S. K., and Arora, V. K.: Model-based assessment of water balance components under different cropping systems in north-west India,  
664 *Agricultural Water Management*, 57, 75-87, [https://doi.org/10.1016/S0378-3774\(02\)00049-5](https://doi.org/10.1016/S0378-3774(02)00049-5), 2002.
- 665 Ji, X. B., Kang, E. S., Chen, R. S., Zhao, W. Z., Zhang, Z. H., and Jin, B. W.: A mathematical model for simulating water balances in cropped  
666 sandy soil with conventional flood irrigation applied, *Agricultural Water Management*, 87, 337-346, <https://doi.org/10.1016/j.agwat.2006.08.011>,  
667 2007.
- 668 Jia, Y., Li, F.-M., Wang, X.-L., and Yang, S.-M.: Soil water and alfalfa yields as affected by alternating ridges and furrows in rainfall harvest in a  
669 semiarid environment, *Field Crops Research*, 97, 167-175, <https://doi.org/10.1016/j.fcr.2005.09.009>, 2006.
- 670 Jiang, Y., Zhang, L., Zhang, B., He, C., Jin, X., and Bai, X.: Modeling irrigation management for water conservation by DSSAT-maize model in  
671 arid northwestern China, *Agricultural Water Management*, 177, 37-45, <https://doi.org/10.1016/j.agwat.2016.06.014> 2016.
- 672 Jinkui, W. U., Yongjian, D., Genxu, W., Yusuke, Y., and Jumpei, K.: Evapotranspiration of Seed Maize Field in Arid Region, *Journal of Irrigation  
673 and Drainage*, 26, 14-17, <https://doi.org/10.3969/j.issn.1672-3317.2007.01.004>, 2007.
- 674 Kallitsari, C., Georgiou, P. E., and Babajimopoulos, C.: Evaluation of Crop Water-Production Functions under Limited Soil Water Availability  
675 with SWBACROS model, in: *Proceedings of the "European Federation for Information Technology in Agriculture, Food and the Environment  
676 World Congress on Computers in Agriculture"*, Prague, July 2011, 585-596, 2011.
- 677 Kang, S., Zhang, L., Liang, Y., Hu, X., Cai, H., and Gu, B.: Effects of limited irrigation on yield and water use efficiency of winter wheat in the  
678 Loess Plateau of China, *Agricultural Water Management*, 55, 203-216, [https://doi.org/10.1016/S0378-3774\(01\)00180-9](https://doi.org/10.1016/S0378-3774(01)00180-9), 2002.
- 679 Katsvairo, T., Cox, W. J., and Van Es, H.: Tillage and Rotation Effects on Soil Physical Characteristics, *Agronomy Journal*, 94, 299-304,  
680 <https://doi.org/10.2134/agronj2002.0299>, 2002.
- 681 Keller, A.: Evapotranspiration and Crop Water Productivity: Making Sense of the Yield-ET Relationship, in: *World Water and Environmental  
682 Resources Congress*, Anchorage, Alaska, United States, 15 May 2005, 1-11, 2005.
- 683 Kirnak, H., and Akpinar, Y.: Performance evaluation of TDR soil moisture sensor, *Agronomy Research*, 14, 428-433, 2016.
- 684 Li, X., Tong, L., Niu, J., Kang, S., Du, T., Li, S., and Ding, R.: Spatio-temporal distribution of irrigation water productivity and its driving factors  
685 for cereal crops in Hexi Corridor, Northwest China, *Agricultural Water Management*, 179, 55-63, <https://doi.org/10.1016/j.agwat.2016.07.010>,  
686 2017.
- 687 Li, Y., Fuchs, M., Cohen, S., Cohen, Y., and Wallach, R.: Water uptake profile response of corn to soil moisture depletion, *Plant Cell and  
688 Environment*, 25, 491-500, <https://doi.org/10.1046/j.1365-3040.2002.00825.x>, 2002.
- 689 Liao, R., Yang, P., Wu, W., and Ren, S.: An Inverse Method to Estimate the Root Water Uptake Source-Sink Term in Soil Water Transport Equation  
690 under the Effect of Superabsorbent Polymer, *Plos One*, 11, <https://doi.org/10.1371/journal.pone.0159936>, 2016.
- 691 Liu, H., and Lin, H.: Frequency and Control of Subsurface Preferential Flow: From Pedon to Catchment Scales, *Soil Science Society of America  
692 Journal*, 79, 362, <https://doi.org/10.2136/sssaj2014.08.0330>, 2015.
- 693 Liu, H., Zhao, W., He, Z., and Liu, J.: Soil moisture dynamics across landscape types in an arid inland river basin of Northwest China, *Hydrological  
694 Processes*, 29, 3328-3341, <https://doi.org/10.1002/hyp.10444>, 2015.
- 695 Liu, W. Z., Hunsaker, D. J., Li, Y. S., Xie, X. Q., and Wall, G. W.: Interrelations of yield, evapotranspiration, and water use efficiency from marginal  
696 analysis of water production functions, *Agricultural Water Management*, 56, 143-151, [http://doi.org/10.1016/S0378-3774\(02\)00011-2](http://doi.org/10.1016/S0378-3774(02)00011-2), 2002.
- 697 Lv, L.: Linking montane soil moisture measurements to evapotranspiration using inverse numerical modeling, Ph.D. dissertation, All Graduate



- 698 Theses and Dissertations, Utah State University, USA, 3323, 2014.
- 699 Muñoz-Carpena, R.: Field Devices For Monitoring Soil Water Content, EDIS, University of Florida Cooperative Extension Service, Institute of  
700 Food and Agricultural Sciences, USA, Open File Rep. 343, 1-24, 2004.
- 701 Musters, P. A. D., and Bouten, W.: Optimum strategies of measuring soil water contents for calibrating a root water uptake model, *Journal of*  
702 *Hydrology*, 227, 273-286, [https://doi.org/10.1016/S0022-1694\(99\)00187-0](https://doi.org/10.1016/S0022-1694(99)00187-0), 2000.
- 703 N. Mbah, C., Nwite, J., Njoku, C., Ibeh, L., and S. Igwe, T.: Physical Properties of an Ultisol under Plastic Film and No-Mulches and Their Effect  
704 on the Yield of Maize, *World Journal of Agricultural Sciences*, 6, 160-165, 2010.
- 705 Naranjo, J. B., Weiler, M., and Stahl, K.: Sensitivity of a data-driven soil water balance model to estimate summer evapotranspiration along a  
706 forest chronosequence, *Hydrology and Earth System Sciences*, 15, 3461, <https://doi.org/10.5194/hess-15-3461-2011>, 2011.
- 707 Odofin, A. J., Egharevba, N. A., Babakutigi, A. N., and Eze, P. C.: Drainage beyond maize root zone in an Alfisol subjected to three land  
708 management systems at Minna, Nigeria, *Journal of Soil Science and Environmental Management*, 3, 216-223,  
709 <https://doi.org/10.5897/JSEM11.143>, 2012.
- 710 Ojha, R., Corradini, C., Morbidelli, R., and Rao, G.: Effective Saturated Hydraulic Conductivity for Representing Field-Scale Infiltration and  
711 Surface Soil Moisture in Heterogeneous Unsaturated Soils Subjected to Rainfall Events, *Water*, 9, 134-151, <https://doi.org/10.3390/w9020134>  
712 2017.
- 713 Peixi, S., Du, M., Zhao, A., and Zhang, X.: Study on water requirement law of some crops and different planting mode in oasis, *Agricultural*  
714 *Research in the Arid Areas*, 20, 79-85, <https://doi.org/10.3321/j.issn:1000-7601.2002.02.019>, 2002.
- 715 Porporato, A., D'Odorico, P., Laio, F., Ridolfi, L., and Rodriguez-Iturbe, I.: Ecohydrology of water-controlled ecosystems, *Advances in Water*  
716 *Resources*, 25, 1335-1348, [https://doi.org/10.1016/S0309-1708\(02\)00058-1](https://doi.org/10.1016/S0309-1708(02)00058-1), 2002.
- 717 Qin, S., Zhang, J., Dai, H., Wang, D., and Li, D.: Effect of ridge-furrow and plastic-mulching planting patterns on yield formation and water  
718 movement of potato in a semi-arid area, *Agricultural Water Management*, 131, 87-94, <https://doi.org/10.1016/j.agwat.2013.09.015>, 2014.
- 719 Quinones, H., and Ruelle, P.: Operative Calibration Methodology of a TDR Sensor for Soil Moisture Monitoring under Irrigated Crops, *Subsurface*  
720 *Sensing Technologies and Applications*, 2, 31-45, <https://doi.org/10.1023/a:1010114109498>, 2001.
- 721 Rahgozar, M., Shah, N., and Ross, M. A.: Estimation of Evapotranspiration and Water Budget Components Using Concurrent Soil Moisture and  
722 Water Table Monitoring, *International Scholarly Research Notices*, 2012, 1-15, <https://doi.org/10.5402/2012/726806>, 2012.
- 723 Read, D. B., Bengough, A. G., Gregory, P. J., Crawford, J. W., Robinson, D., Scrimgeour, C. M., Young, I. M., Zhang, K., and Zhang, X.: Plant  
724 roots release phospholipid surfactants that modify the physical and chemical properties of soil, *New Phytologist*, 157, 315-326,  
725 <https://doi.org/10.1046/j.1469-8137.2003.00665.x>, 2003.
- 726 Rice, R. C., Bowman, R. S., and Jaynes, D. B.: Percolation of Water Below an Irrigated Field, *Soil Science Society of America Journal*, 50, 855-  
727 859, <https://doi.org/10.2136/sssaj1986.03615995005000040005x>, 1986.
- 728 Rong, Y.: Estimation of maize evapotranspiration and yield under different deficit irrigation on a sandy farmland in Northwest China, *African*  
729 *Journal of Agricultural Research*, 7, 4698-4707, <https://doi.org/10.5897/AJAR11.1213>, 2012.
- 730 Séré, G., Ouvrard, S., Magnenet, V., Pey, B., Morel, J. L., and Schwartz, C.: Predictability of the Evolution of the Soil Structure using Water Flow  
731 Modeling for a Constructed Technosol, *Vadose Zone J.*, 11, 59-75, <https://doi.org/10.2136/vzj2011.0069> 2012.
- 732 Salazar, O., Wesström, I., and Joel, A.: Evaluation of DRAINMOD using saturated hydraulic conductivity estimated by a pedotransfer function  
733 model, *Agricultural Water Management*, 95, 1135-1143, <https://doi.org/10.1016/j.agwat.2008.04.011>, 2008.
- 734 Salem, H. M., Valero, C., Muñoz, M. Á., Rodríguez, M. G., and Silva, L. L.: Short-term effects of four tillage practices on soil physical properties,  
735 soil water potential, and maize yield, *Geoderma*, 237, 60-70, <https://doi.org/10.1016/j.geoderma.2014.08.014>, 2015.
- 736 Schelde, K., Ringgaard, R., Herbst, M., Thomsen, A., Friberg, T., and Sogaard, H.: Comparing Evapotranspiration Rates Estimated from  
737 Atmospheric Flux and TDR Soil Moisture Measurements, *Vadose Zone J.*, 10, 78, <https://doi.org/10.2136/vzj2010.0060>, 2011.
- 738 Schneider, C. L., Attinger, S., Delfs, J. O., and Hildebrandt, A.: Implementing small scale processes at the soil-plant interface - the role of root  
739 architectures for calculating root water uptake profiles, *Hydrology and Earth System Sciences*, 14, 279-289, [https://doi.org/10.5194/hess-14-279-](https://doi.org/10.5194/hess-14-279-2010)  
740 2010, 2010.
- 741 Selle, B., Minasny, B., Bethune, M., Thayalakumaran, T., and Chandra, S.: Applicability of Richards' equation models to predict deep percolation  
742 under surface irrigation, *Geoderma*, 160, 569-578, <https://doi.org/10.1016/j.geoderma.2010.11.005>, 2011.
- 743 Shah, N., Ross, M., and Trout, K.: Using Soil Moisture Data to Estimate Evapotranspiration and Development of a Physically Based Root Water  
744 Uptake Model, *Evapotranspiration-Remote Sensing and Modeling*, Dr. Ayse Irmak (Ed.), IntechOpen, <https://doi.org/10.5772/18040>, 2012.



- 745 Sharma, H., Shukla, M. K., Bosland, P. W., and Steiner, R.: Soil moisture sensor calibration, actual evapotranspiration, and crop coefficients for  
746 drip irrigated greenhouse chile peppers, *Agricultural Water Management*, 179, 81-91, <https://doi.org/10.1016/j.agwat.2016.07.001>, 2017.
- 747 Sławiński, Sobczuk, H., Stoffregen, H., Walczak, R., and Wessolek, G.: Effect of data resolution on soil hydraulic conductivity prediction, *Journal*  
748 *of Plant Nutrition and Soil Science*, 165, 45–49, [https://doi.org/10.1002/1522-2624\(200202\)165:1<45::AID-JPLN45>3.0.CO;2-I](https://doi.org/10.1002/1522-2624(200202)165:1<45::AID-JPLN45>3.0.CO;2-I), 2002.
- 749 Sr, H. J. C., Grimm, N. B., Gosz, J. R., and Seastedt, T. R.: The US Long Term Ecological Research Program, *Bioscience*, 53, 21-32,  
750 [https://doi.org/10.1641/0006-3568\(2003\)053\[0021:TULTER\]2.0.CO;2](https://doi.org/10.1641/0006-3568(2003)053[0021:TULTER]2.0.CO;2), 2003.
- 751 Srivastava, R. K., Panda, R. K., and Halder, D.: Effective crop evapotranspiration measurement using time-domain reflectometry technique in a  
752 sub-humid region, *Theoretical and Applied Climatology*, 129, 1211-1225, <https://doi.org/10.1007/s00704-016-1841-7>, 2017.
- 753 Su, P. X., Xie, T. T., and Ding, S. S.: Water requirement regularity in Linze jujube (*Ziziphus jujuba* Mill. var. *inermis* Rehd. cv. *Linze jujube*) and  
754 jujube/crop complex systems in Linze oasis, *Chinese Journal of Eco-Agriculture*, 18, 334-341, <https://doi.org/10.3724/SP.J.1011.2010.00334>, 2010.
- 755 Su, Y., Yang, X., and Yang, R.: Effect of Soil Texture in Unsaturated Zone on Soil Nitrate Accumulation and Groundwater Nitrate Contamination  
756 in a Marginal Oasis in the Middle of Heihe River Basin, *Environmental Science*, 35, 3683-3691, <https://doi.org/10.13227/j.hjlx.2014.10.007>, 2014.
- 757 Suleiman, A. A., and Hoogenboom, G.: Comparison of Priestley-Taylor and FAO-56 Penman-Monteith for daily reference evapotranspiration  
758 estimation in Georgia, *Journal of Irrigation and Drainage Engineering*, 133, 175-182, [https://doi.org/10.1061/\(asce\)0733-9437\(2007\)133:2\(175\)](https://doi.org/10.1061/(asce)0733-9437(2007)133:2(175)),  
759 2007.
- 760 Sun, H. R., Rui-Xin, W. U., Pin-Hong, L. I., Shao, S., Lin-Lu, Q. I., and Han, J. G.: Rooting Depth of Alfalfa, *Acta Agrestia Sinica*, 16, 307-312,  
761 <https://doi.org/10.11733/j.issn.1007-0435.2008.03.019>, 2008.
- 762 Topp, G. C., Davis, J., and Annan, A. P.: Electromagnetic determination of soil water content: Measurements in coaxial transmission lines, *Water*  
763 *resources research*, 16, 574-582, <https://doi.org/10.1029/WR016i003p00574>, 1980.
- 764 Wang, K., and Dickinson, R. E.: A review of global terrestrial evapotranspiration: Observation, modeling, climatology, and climatic variability,  
765 *Reviews of Geophysics*, 50.2, <https://doi.org/10.1029/2011RG000373>, 2012.
- 766 Wang, P., Yu, J., Pozdniakov, S. P., Grinevsky, S. O., and Liu, C.: Shallow groundwater dynamics and its driving forces in extremely arid areas: a  
767 case study of the lower Heihe River in northwestern China, *Hydrological Processes*, 28, 1539-1553, <https://doi.org/10.1002/hyp.9682>, 2014.
- 768 Wright, J. L.: Way Sought to Measure Irrigation Water Needs, *Crops and Soils Magazine*, 23, 20-211, 1971.
- 769 Wu, X., Zhou, J., Wang, H., Li, Y., and Zhong, B.: Evaluation of irrigation water use efficiency using remote sensing in the middle reach of the  
770 Heihe river, in the semi-arid Northwestern China, *Hydrological Processes*, 29, 2243-2257, <https://doi.org/10.1002/hyp.10365>, 2015.
- 771 Yang, B., Wen, X., and Sun, X.: Irrigation depth far exceeds water uptake depth in an oasis cropland in the middle reaches of Heihe River Basin,  
772 *Scientific Reports*, 5, 15206, <https://doi.org/10.1038/srep15206>, 2015.
- 773 Yang, J., Mao, X., Wang, K., and Yang, W.: The coupled impact of plastic film mulching and deficit irrigation on soil water/heat transfer and water  
774 use efficiency of spring wheat in Northwest China, *Agricultural Water Management*, 201, 232-245, <https://doi.org/10.1016/j.agwat.2017.12.030>,  
775 2018a.
- 776 Yang, X., Yu, Y., and Li, M.: Estimating soil moisture content using laboratory spectral data, *Journal of Forestry Research*, 1-8,  
777 <https://doi.org/10.1007/s11676-018-0633-6>, 2018b.
- 778 Yong, H., Hou, L., Hong, W., Hu, K., and Mcconkey, B.: A modelling approach to evaluate the long-term effect of soil texture on spring wheat  
779 productivity under a rain-fed condition, *Scientific Reports*, 4, 5736, <https://doi.org/10.1038/srep05736>, 2014.
- 780 You, D. B., Wang, J. L., Ming-Qiang, L., and Hua, Q. I.: Evapotranspiration of Maize Field in Irrigation Area in Heihe Middle Reaches Using the  
781 Penman-Monteith Method, *Acta Agriculturae Boreali-Sinica*, 139-145, <https://doi.org/10.7668/hbxb.2015.S1.025>, 2015.
- 782 Young, M. H., Wierenga, P. J., and Mancino, C. F.: Monitoring Near-Surface Soil Water Storage in Turfgrass using Time Domain Reflectometry  
783 and Weighing Lysimetry, *Soil Science Society of America Journal*, 61, 1138-1146, <https://doi.org/10.2136/sssaj1997.03615995006100040021x>,  
784 1997.
- 785 Zhang, Y. L., Wang, F. X., Shock, C. C., Yang, K. J., Kang, S. Z., Qin, J. T., and Li, S. E.: Influence of different plastic film mulches and wetted  
786 soil percentages on potato grown under drip irrigation, *Agricultural Water Management*, 180, 160-171, <https://doi.org/10.1016/j.agwat.2016.11.018>,  
787 2017.
- 788 Zhang, Y., Kendy, E., Qiang, Y., Changming, L., Yanjun, S., and Hongyong, S.: Effect of soil water deficit on evapotranspiration, crop yield, and  
789 water use efficiency in the North China Plain, *Agricultural Water Management*, 64, 107-122, [https://doi.org/10.1016/s0378-3774\(03\)00201-4](https://doi.org/10.1016/s0378-3774(03)00201-4),  
790 2004.
- 791 Zhang, Y. Y., Wu, P. T., Zhao, X. N., and Zhao, W. Z.: Measuring and modeling two-dimensional irrigation infiltration under film-mulched furrows,



- 792 Sciences in Cold and Arid Regions, 8, 419-431, <https://doi.org/10.3724/SP.J.1226.2016.00419>, 2016.
- 793 Zhao, L., and Ji, X.: Quantification of Transpiration and Evaporation over Agricultural Field Using the FAO-56 Dual Crop Coefficient Approach-  
794 A case study of the maize field in an oasis in the middle stream of the Heihe River Basin in Northwest China, *Scientia Agricultura Sinica*, 43,  
795 4016-4026, <https://doi.org/10.3864/j.issn.0578-1752.2010.19.014>, 2010.
- 796 Zhao, L., and Zhao, W.: Water balance and migration for maize in an oasis farmland of northwest China, *Chinese Science Bulletin*, 59, 4829-4837,  
797 <https://doi.org/10.1007/s11434-014-0482-4>, 2014.
- 798 Zhao, L., Zhao, W., and Ji, X.: Division between transpiration and evaporation, and crop water consumption over farmland within oases of the  
799 middlestream of Heihe River basin, Northwestern China, *Acta Ecologica Sinica*, 35, 1114-1123, <https://doi.org/10.5846/stxb201304220778>, 2015.
- 800 Zhao, L., He, Z., Zhao, W., and Yang, Q.: Extensive investigation of the sap flow of maize plants in an oasis farmland in the middle reach of the  
801 Heihe River, Northwest China, *Journal of Plant Research*, 129, 841-851, <https://doi.org/10.1007/s10265-016-0835-y>, 2016.
- 802 Zhao, W., Liu, B., and Zhang, Z.: Water requirements of maize in the middle Heihe River basin, China, *Agricultural Water Management*, 97, 215-  
803 223, <https://doi.org/10.1016/j.agwat.2009.09.011>, 2010.
- 804 Zhao, W., and Chang, X.: The effect of hydrologic process changes on NDVI in the desert-oasis ecotone of the Hexi Corridor, *Science China-Earth  
805 Sciences*, 57, 3107-3117, <https://doi.org/10.1007/s11430-014-4927-z>, 2014.
- 806 Zhou, H., Zhao, W., and Zhang, G.: Varying water utilization of Haloxylon ammodendron plantations in a desert-oasis ecotone, *Hydrological  
807 Processes*, 31, 825-835, <https://doi.org/10.1002/hyp.11060>, 2017.
- 808 Zotarelli, L., Dukes, M. D., Morgan, and T., K.: Interpretation of Soil Moisture Content to Determine Soil Field Capacity and Avoid Over-Irrigating  
809 Sandy Soils Using Soil Moisture Sensors, *Agricultural and Biological Engineering*, 2016.
- 810 Zou, M., Niu, J., Kang, S., Li, X., and Lu, H.: The contribution of human agricultural activities to increasing evapotranspiration is significantly  
811 greater than climate change effect over Heihe agricultural region, *Scientific Reports*, 7, 8805, <https://doi.org/10.1038/s41598-017-08952-5>, 2017.
- 812 Zuo, Qiang, Zhang, and Renduo: Estimating root-water-uptake using an inverse method *Soil Science*, 167, 561-571,  
813 <https://doi.org/10.1097/00010694-200209000-00001>, 2002.